AGU PUBLICATIONS

Water Resources Research

RESEARCH ARTICLE
10.1002/2016WR019208

Variational assimilation of streamflow data in distributed flood forecasting

Giulia Ercolani [1] and Fabio Castelli[1]

[1]Department of Civil and Environmental Engineering, University of Florence, Florence, Italy

Key Points:
- Variational assimilation of streamflow data from multiple sites in a distributed hydrologic model
- The proposed DA scheme is evaluated to be usable operationally through many hindcast experiments
- Performances vary with OL accuracy, compatibility between model and event, initial soil saturation

Correspondence to:
G. Ercolani,
giulia.ercolani@dicea.unifi.it

Citation:
Ercolani, G., and F. Castelli (2017), Variational assimilation of streamflow data in distributed flood forecasting, *Water Resour. Res.*, *53*, 158–183, doi:10.1002/2016WR019208.

Received 13 MAY 2016
Accepted 28 NOV 2016
Accepted article online 17 DEC 2016
Published online 11 JAN 2017

Abstract Data assimilation has the potential to improve flood forecasting. However, research efforts are still needed for an effective development of assimilation schemes suitable for operational usage, especially in case of distributed hydrologic models. This work presents a new assimilation system of streamflow data from multiple locations in a distributed hydrologic model. The system adopts a mixed variational-Monte Carlo approach, and is here tested with the hydrologic model MOBIDIC, that is part of the operational flood forecasting chain for Arno river in central Italy. The main objective of the work is to evaluate the actual gain that the system can lead to flood predictions in a real-time operational usage. Accordingly, a specifically designed assessment strategy is employed. It is based on several hindcast experiments that include both high flow and false alarm events in the period 2009–2014 in Arno river basin. Results show that the assimilation system can significantly increase the accuracy of flow predictions in respect to open loop simulations in both cases. Specific performances depend on location and event, but in the majority of cases the error on predicted peak flow is reduced of more than 50% with a lead time of around 10 h. The analysis reveals also that the structure of the hydrologic model, the coherence between observations at various sites, and the initial watershed saturation level, considerably affect the obtainable performances. Conditions that may lead to a worsening of open loop predictions are identified and discussed.

1. Introduction

Accurate and reliable streamflow predictions are fundamental for effective early warning systems, which are crucial in reducing floods impact [*UNISDR*, 2002; *Carsell et al.*, 2004; *Molinari and Handmer*, 2011; *Pappenberger et al.*, 2015] and are increasingly used worldwide in flood risk management [*Pagano et al.*, 2014]. Data assimilation is recognized to be a valuable tool to gain accuracy in streamflow predictions [*Liu et al.*, 2012]. Basically, data assimilation combines observations and numerical models to enhance states and parameters estimation. It is an established practice in operational meteorology, where it represents a crucial step for numerical weather predictions and reanalysis [*Kalnay*, 2003]. Numerous studies demonstrated its potential also in hydrology, using different methods and observations. Typically employed observations are in-situ measurements of streamflow [e.g., *Seo et al.*, 2003; *Vrugt et al.*, 2006; *Komma et al.*, 2008; *Clark et al.*, 2008; *Seo et al.*, 2009; *Rakovec et al.*, 2012; *Moradkhani et al.*, 2012; *McMillan et al.*, 2013; *Coustau et al.*, 2013; *Abaza et al.*, 2014; *Noh et al.*, 2014; *Rafieeinasab et al.*, 2014; *Mazzoleni et al.*, 2015; *Li et al.*, 2015; *Rakovec et al.*, 2015] and satellite retrievals of soil moisture [e.g., *Pauwels et al.*, 2001; *Reichle et al.*, 2007; *Brocca et al.*, 2010, 2012; *Li et al.*, 2012; *Sahoo et al.*, 2013; *Laiolo et al.*, 2015], snow cover [e.g., *Clark et al.*, 2006; *Liston and Hiemstra*, 2008; *Su et al.*, 2010; *De Lannoy et al.*, 2012], land surface temperature [e.g., *Caparrini et al.*, 2004a, 2004b; *Sini et al.*, 2008; *Reichle et al.*, 2010; *Campo et al.*, 2013], evapotranspiration [e.g., *Schuurmans et al.*, 2003; *Pipunic et al.*, 2008; *Irmak and Kamble*, 2009; *Schuurmans et al.*, 2011], and vegetation characteristics [e.g., *Fang et al.*, 2011; *Ines et al.*, 2013]. When the assimilation procedure aims at improving streamflow forecasting, in-situ discharge data are more commonly used than satellite products of soil moisture, especially if the application is in real time. The main reason is that it is more straightforward to assimilate the same variable which is forecast. In addition, the choice is also due to the fact that the temporal resolution of discharge measurements is superior, with hourly or subhourly data versus typical much longer revisit times of satellites used operationally for soil moisture retrieval. A frequent strategy is to employ streamflow observations for model states updating (usually states of soil moisture and of surface or river flow) [e.g., *Komma et al.*, 2008; *Clark et al.*, 2008; *Chen et al.*, 2012; *Noh et al.*, 2013; *Li et al.*, 2015]. However, some studies indicate that a potentially successful approach is to combine states update with

parameters estimation [e.g., *Vrugt et al*., 2006; *Seo et al*., 2003, 2009]. This allows to better deal with possible structural and parametric errors of the model. The most common approaches adopted in hydrologic data assimilation are Kalman filters (linear, extended, and ensemble Kalman filter), particle filters and variational methods. A comprehensive analysis of these methods in the hydrological context is provided in *Liu and Gupta* [2007], and *Reichle* [2008]. Ensemble Kalman filter [*Evensen*, 1994] can be considered the most common technique. Its popularity is due mainly to the fact it can deal efficiently with non linear models and it is flexible and easy to use, as well as straightforward to implement irrespective of model specific characteristics [e.g., *Clark et al*., 2008; *Komma et al*., 2008; *Pauwels and De Lannoy*, 2009; *Xie and Zhang*, 2010; *Rakovec et al*., 2012; *McMillan et al*., 2013]. Analogous considerations about flexibility and straightforward implementation are appropriate also for particle filters, although their rationale and functioning differ substantially from ensemble Kalman filter (see, for instance, *Moradkhani et al*. [2005], *Salamon and Feyen* [2009], or *Arulampalam et al*. [2002] for details about the technique). Furthermore, particle filters do not require the assumption of Gaussian state-space model as ensemble Kalman filter does. Given this advantage, as well as the refining of specific techniques, particle filtering is increasingly employed in hydrologic data assimilation [e.g., *Weerts and El Serafy*, 2006; *Noh et al*., 2011; *Moradkhani et al*., 2012; *DeChant and Moradkhani*, 2011, 2012; *Pasetto et al*., 2012; *Yan and Moradkhani*, 2016]. Variational methods are less diffused in hydrology, as they require the not straightforward derivation of an adjoint model. However, they are less computationally expensive and more flexible in case of complex systems [*Reichle et al*., 2001; *Liu and Gupta*, 2007; *McMillan et al*., 2013] and, since they use observations inside an assimilation window all at once, are less subjected to overshoots in corrections, i.e., they are smoothers [*Reichle*, 2008].

Despite the increasing attention that data assimilation is gaining in hydrology, the transfer of research results into operational systems is still considered insufficient [*Liu et al*., 2012], with most of the literature focusing on theoretical advances and synthetic tests [e.g., *Andreadis et al*., 2007; *Reichle et al*., 2008; *Crow and Ryu*, 2009; *Kumar et al*., 2009]. However, in the last years, synthetic tests have contributed, together with real case studies, to understand the potential and the challenges in using data assimilation with distributed hydrologic schemes [*Komma et al*., 2008; *Clark et al*., 2008; *Salamon and Feyen*, 2009; *Brocca et al*., 2010; *Lee et al*., 2011, 2012; *Yan and Moradkhani*, 2016]. Indeed, several issues arise when dealing with a distributed approach instead of lumped, and research efforts are needed to properly address them. The main troubles are the large dimensionality of the inverse problem, eventually causing overfitting in the update, the complex topology of domains such as surface drainage and river network, and model governed by different equations with a nonlinear and discontinuous structure [*Clark et al*., 2008; *Lee et al*., 2011, 2012; *Rakovec et al*., 2012]. Despite the relevant advances made, in the operational practice data assimilation is included in hydrologic forecasting mainly with lumped models [*Seo et al*., 2009; *Chen et al*., 2012]. A noticeable exception is the system running at Météo France. It uses the Best Linear Unbiased Estimator (BLUE) with streamflow observations at multiple locations to update soil moisture states in a distributed hydrologic model that is forced by an ensemble of meteorological inputs. The inclusion of streamflow assimilation in the operational forecasting chain was presented and tested in *Thirel et al*. [2010a, 2010b] over the whole France. Results demonstrated a great potential of the assimilation scheme in a synthetic experiment, where also streamflows at not assimilated locations improved. Performances slightly reduced in forecasting mode using real data, but confirmed the value of the system. *Coustau et al*. [2015] completed the evaluation adopting entirely the operational setting, which includes to employ observations only from a limited number of gauge stations. The results highlighted the fundamental role of stations spatial distribution for a successful assimilation. However, the improvement of both the assimilation strategy and the hydrologic model is envisaged. In particular, it is wished to overcome the limitations related to the usage of a linearized observation operator in the assimilation. Furthermore, among the few studies that are operationally-oriented for distributed schemes, only a small number performs a specific evaluation of the assimilation system that is actually useful to assess the benefit in terms of flood early warning. Such evaluation should be event-based, i.e., statistical indexes of performance should be computed on any flood event, or, better, on any event that is relevant in terms of either streamflow or rainfall (i.e., also relevant rainfall events which do not cause a significant rise of discharge in the river network should be examined). Instead, many studies [e.g., *Thirel et al*., 2010a, 2010b; *Rakovec et al*., 2012; *McMillan et al*., 2013; *Coustau et al*., 2015] evaluate the assimilation system continuously over long periods, i.e., they compute performance indexes on time series of streamflow that extend over several months or years, and hence include numerous dry periods. In addition, the assessment should focus on improvements in predictions of the single hydrograph and on specific skills that are

fundamental for flood warning, such as peak flow. Moreover, lead time should be taken into account. *Komma et al*. [2008] and *Coustau et al*. [2013] are studies that adopt an event-based approach for the verification of the proposed assimilation systems. However, their verification strategies differ slightly, and could be integrated to assure a comprehensive evaluation that is preparatory for an operational usage in flood early warning systems. Only *Komma et al*. [2008] include in the analysis the dependence of results on lead time. Conversely, *Coustau et al*. [2013] examine a larger number of events (12 cases), showing that the performances of the assimilation scheme can change significantly in function of the specific case. Moreover, both studies assimilate streamflow data and quantify improvements in predictions solely at the basin outlet, although they both employ a distributed hydrologic model. Hence, issues that could rise from using spatially distributed information, as well as the possible spatial variability of performances, are not analyzed.

Our work presents a new data assimilation system for streamflow observations at multiple locations in a distributed hydrologic model, and aims at evaluating whether and to which extent this system could enhance flood forecasting in the operational practice. The developed system is a mixed variational-Monte Carlo method. It represents a novel approach that could overcome challenges related to the derivation of an adjoint model for modular schemes with strong threshold nonlinearities. Thanks to this mixed approach, the system updates efficiently initial river flow and soil moisture, as well as a parameter related to infiltration processes, on a distributed basis. For the assessment of performances, we employ an event-based approach, since we are specifically interested in enhancing predictions for flood early warning. We examine a large number of events (16) with different characteristics. In fact, the assimilation system is intended to be employed operationally, and we need to verify its behavior under the large variety of conditions that are encountered in a real-time usage. Accordingly, both high flow and false alarms (relevant rainfall accumulation but relatively low river flows) cases are included in the analysis. Furthermore, the dependence of results from lead time is investigated, being a crucial feature that could determine the usefulness of the assimilation scheme in terms of early warning. Both the assimilation and the corresponding evaluation of performances are performed at multiple locations, increasing the completeness of the analysis. All these characteristics are rarely present simultaneously in an assessment strategy. However, they are fundamental to verify exhaustively the operational usability of an assimilation framework for improvement of flood forecasting, as our work is intended to. Hence, this study contributes significantly to the transfer of research activities to the operational practice, which is still considered insufficient especially for spatially distributed systems (both model and assimilation scheme). Besides the previous facts, the following specific points merit attention in regard to the few existing studies on the use of the variational approach to assimilate streamflow data at multiple gauge stations in distributed hydrologic models [e.g., *Lee et al*., 2011, 2012]: (i) the results obtained so far are still controversial, and significantly dependent on hydrologic model capacity to predict streamflow in the basin of interest, as well as on the details of the assimilation strategy, which in turn are related to the peculiarities of the hydrologic model (in the above studies, the gridded Sacramento Soil Moisture Accounting and kinematic-wave routing modules that are part of the National Weather Service Hydrology Laboratorys Research Distributed Hydrologic Model); (ii) a fine spatial resolution (below kilometer scale), capable of fully resolving the hillslope and drainage structure, is used here for the first time in a variational assimilation context.

The new assimilation system is tested with the hydrologic model MOBIDIC (MOdello di Bilancio Idrologico Distribuito e Continuo). MOBIDIC runs operationally at the hydrologic service of Tuscany region, Italy, for flood forecasting and water resources management purposes. We analyze the developed framework in 16 hindcast experiments that include both high flow and false alarm events in the period 2009–2014. Experiments are run with a high spatial resolution. The area of study is Arno river basin, which is the main catchment of Tuscany region.

The remainder of the paper is organized as follows. Sections 2 and 3 describe the hydrological model MOBIDIC and the developed assimilation system respectively. Section 4 illustrates the area of study and the setup of the hindcast experiments. Results are presented in section 5, and conclusions are drawn in section 6.

2. The Hydrologic Model MOBIDIC

MOBIDIC (MOdello di Bilancio Idrologico DIstribuito e Continuo) is a physically-based hydrologic model that runs operatively at the hydrologic service of Tuscany region (Servizio Idrologico Regionale, Regione

Toscana) for floods forecasting and water resources management purposes. It works at the watershed scale, and estimates hydrologic fluxes and states in surface water bodies (both river network and reservoirs), soil-vegetation system and subsurface layer [*Campo et al*., 2006; *Castelli et al*., 2009; *Yang et al*., 2014a, 2014b]. It is continuous in time and spatially distributed, with horizontal discretization based on a square grid DEM (Digital Elevation Model).

MOBIDIC solves water and energy balance simultaneously in the soil-vegetation subsystem. Water dynamics are represented through a computationally efficient scheme, that was recently enhanced by *Castillo et al*. [2015]. It discretizes soil vertically with one single layer, that is conceptually subdivided into two nonlinear reservoirs, the capillary and gravitational compartments. They represent, respectively, smaller pores that hold water through capillary forces and larger pores that drains under gravity. Accordingly, the maximum storage capacity of the gravitational reservoir ($W_{g,\max}$) may be parametrized as the maximum water content above field capacity, and that of the capillary reservoir ($W_{c,\max}$) as the difference between field capacity and wilting point. The two compartments regulate different hydrologic fluxes. *Castillo et al*. [2015] demonstrated that this dual-pore storage model captures the essential local-scale soil moisture dynamics, and provides results that are comparable to those obtained with a numerical solver of Richards equation. For each cell of the domain, the time evolution of gravitational (W_g) and capillary water (W_c) is driven by:

$$\frac{dW_g}{dt} = I + Q_{L,up} - Q_{as} - Q_{per} - Q_{L,down} \tag{1}$$

$$\frac{dW_c}{dt} = Q_{as} + Q_{cap} - E_3 \tag{2}$$

where I is infiltration, $Q_{L,up}$ is incoming hypodermic flow from uphill cells, Q_{as} is absorption of water from gravitational to capillary reservoir, Q_{per} is percolation, $Q_{L,down}$ is outgoing hypodermic flow toward the downhill cell, Q_{cap} is capillary rise from shallow water table and E_3 is evapotranspiration. Water balance includes two additional reservoirs, the canopy and surface runoff compartments. The first one accounts for interception of rainfall by plants canopy, and the second one for temporary storage in runoff. Their water content, W_p and W_s respectively, evolves in time in accordance with:

$$\frac{dW_p}{dt} = P - T - E_1 \tag{3}$$

$$\frac{dW_s}{dt} = R_H + R_D - R_{down} - E_2 \tag{4}$$

where P is precipitation, T is throughfall, R_H is Horton runoff, R_D is Dunne runoff, R_{down} is outgoing runoff toward the downhill cell, E_1 and E_2 are direct evaporation from canopy and surface water respectively. Water contents are here expressed as volume per unit area [L], and fluxes as volume per area and time unit [LT^{-1}]. Fluxes between the four conceptual reservoirs are described in the following. Infiltration provides water to the gravitational reservoir. It is limited in rate by soil hydraulic conductivity K_s [LT^{-1}], and in volume by the maximum storage capacity of the gravitational compartment. Accordingly, Horton and Dunne runoff may be generated. Regarding Horton runoff, a stochastic approach is adopted to take into account the intermittent nature of precipitation. At each time step, the expected value of the infiltration rate is computed assuming that rainfall is a random variable with an exponential distribution [*Castelli*, 1996].

$$I = \begin{cases} (T + R_{up})\left[1 - \exp\left(-\dfrac{(1-f_0)K_s K^+}{T + R_u p}\right)\right] & \text{if } W_g \le W_{g,\max} \\ 0 & \text{if } W_g > W_{g,\max} \end{cases} \tag{5}$$

where R_{up} is incoming runoff from uphill cells and f_0 is a parameter representing rainfall intermittence (for details, see *Castelli* [1996]). Moreover, K^+ [−] is a parameter accounting for augmented infiltration rate before surface ponding. This brings back the role of the capillary compartment which may dominate the early stage of infiltration. K^+ is then assumed to be dependent on the level of saturation of capillary soil. Both percolation toward groundwater and downhill hypodermic flow are parametrized as linearly dependent on gravitational water content:

$$Q_{per} = \gamma \cdot W_g \tag{6}$$

$$Q_{L,down} = \beta \cdot W_g \tag{7}$$

where γ and β are the corresponding empirical rate coefficients $[T^{-1}]$. Moreover, water leaves the gravitational reservoir through an absorption flux that feeds the capillary compartment. Absorption is considered linearly dependent on a bulk suction head through an empirical rate coefficient k $[T^{-1}]$:

$$Q_{as} = k \cdot (W_{c,\max} - W_c) \tag{8}$$

The capillary reservoir may receive water also through capillary rise when a shallow water table is present. The flux is modeled according to *Salvucci* [1993]:

$$Q_{cap} = \frac{K_s[(d_w/\psi_b)^{-n} - (\psi/\psi_b)^{-n}]}{1 + (\psi/\psi_b)^{-n} + (n-1)(d_w/\psi_b)^{-n}} \tag{9}$$

where d_w [L] is the mean distance between the water table and the unsaturated soil layer, ψ [L] is the soil matric potential (computed following *Brooks and Corey* [1964]), ψ_b [L] is the bubbling pressure, and n $[-]$ is the product of Brooks-Corey pore size distribution index and pore-size disconnectedness index. Outgoing runoff toward the downhill cell is evaluated as linearly dependent from surface water content through a kinematic parameter $\hat{\alpha}$:

$$R_{down} = \hat{\alpha} \cdot W_s \tag{10}$$

$$\hat{\alpha} = \alpha \cdot \frac{\sqrt{i}}{\overline{\sqrt{i}}} \tag{11}$$

where α $[T^{-1}]$ is a rate coefficient for runoff, i $[-]$ is the topographic slope and $\bar{\cdot}$ indicates averaging over the cells of the basin. Finally, throughfall is computed as excess over the maximum storage of the canopy reservoir:

$$T = \begin{cases} P - W_{p,\max}/\Delta t & \text{if } W_p > W_{p,\max} \\ 0 & \text{if } W_p \leq W_{p,\max} \end{cases} \tag{12}$$

Additional specifications about fluxes computation can be found in *Castelli et al.* [2009] and *Castillo et al.* [2015].

Evapotranspiration is subtracted from canopy, surface and capillary soil reservoirs according to their water availability and on the basis of potential evapotranspiration, that is computed through the surface energy balance:

$$R_n - G = H + LE \tag{13}$$

where R_n is the net radiation available at the surface, G is heat flux into soil (positive downward), H and LE are surface turbulent fluxes of sensible and latent heat respectively (positive upward). The turbulent fluxes, in (W m^{-2}), are computed employing a bulk formulation for heat transfer:

$$H = \rho_a C_p C_H U (T_s - T_a) \tag{14}$$

$$LE = \rho_a L C_H U (q_s - q_a) \tag{15}$$

where ρ_a (kg m^{-3}) is air density, C_p (J kg^{-1} K^{-1}) is air specific heat at constant pressure, L (J kg^{-1}) is latent heat of vaporization, U (m s^{-1}) is wind speed, T_s and T_a (K) are temperatures of land surface and air, q_s and q_a (kg kg^{-1}) are specific humidities of surface and air, and C_H (-) is the bulk transfer coefficient for heat. It includes both surface roughness and atmospheric stability effects [*Van den Hurk and Holtslag*, 1997]. Potential (energy-limited) evapotranspiration is computed first. The energy balance is coupled with the 1-D equation of heat diffusion into soil:

$$\rho_s C_s \frac{\partial T}{\partial t} = \frac{\partial}{\partial z}\left(k \frac{\partial T}{\partial z}\right) \tag{16}$$

where ρ_s (kg m^{-3}) is soil density, C_s (J K^{-1} kg^{-1}) is soil heat capacity, k (W m^{-1} K^{-1}) is soil thermal conductivity, and T (K) is soil temperature. Equation (16) is integrated forward in time employing a three-point

vertical discretization. As lower boundary condition a constant temperature is imposed, while the top boundary condition is:

$$k\left.\frac{\partial T}{\partial z}\right|_{z=0} = -G \tag{17}$$

Actual evapotranspiration is computed taking into account water availability in canopy, surface and capillary soil reservoirs, and it is used to solve again the energy balance and hence to obtain the actual update of land surface temperature T_s. This coupling between energy and water balance gives the possibility (not used here) to assimilate land surface temperature observations for the improvement of soil moisture estimation.

Groundwater dynamics may be modeled through 2-D Dupuit approximation or as a linear reservoir. In both approaches an explicitly interaction between subsurface and surface is included. The latter method is employed in the present work, focused on head dynamics in a watershed where groundwater contribution to high flows is negligible.

The hydrographic network is represented in vector form, as inferred from "blue lines maps," and channels are treated as cylindrical. Rivers are fed by surface runoff and base flow from groundwater. Three options are available for flow routing through the network, i.e., lag approach, Muskingum-Cunge method and cascade of liner reservoirs. The assimilation scheme is developed for the latter method, that represents an optimal compromise between complexity and representativeness of the physical process. Hence, the system of governing equation here considered for flow routing is:

$$\frac{d\boldsymbol{Q}(t)}{dt} = \boldsymbol{A}[\boldsymbol{q_L}(t) + \boldsymbol{U}\boldsymbol{Q}(t) - \boldsymbol{Q}(t)] = \boldsymbol{F}(\boldsymbol{A}, \boldsymbol{Q}(t), \boldsymbol{q_L}(t)) \tag{18}$$

where, with a network composed by n reaches, $\boldsymbol{Q}(t) \in \mathbb{R}^n$ are the discharges exiting each reach at time t, $\boldsymbol{q_L}(t) \in \mathbb{R}^n$ are the lateral inflows (surface runoff plus groundwater flow) at the same instant, and $\boldsymbol{A} \in \mathbb{R}^{n\times n}$ is a diagonal matrix with the inverse of the characteristic time of each river on the diagonal, which are assumed to be constant in time. Lastly, $\boldsymbol{U} \in \mathbb{R}^{n\times n}$ is a binary matrix accounting for the network topology. Each row of $\boldsymbol{U}$ corresponds to a river reach, with 1 in the columns of its tributaries and 0 elsewhere. The evolution of the state $\boldsymbol{Q}(t)$ depends on its initial condition, parameters $\boldsymbol{A}$ and time-varying input $\boldsymbol{q_L}(t)$.

3. The Assimilation Scheme

The assimilation system is based on a variational approach, since it demands less restrictive hypothesis than Kalman and Monte Carlo filters and smoothers. The scheme aims at enhancing flood forecasting through the assimilation of river flow observations at multiple locations. Hence, an adjoint model for MOBIDIC module of flow routing is derived. The scheme will provide estimates of initial conditions and of parameters involved in flow formation processes.

3.1. Adjoint Model of Flow Routing in the River Network

Following a classical variational approach [e.g., *Castelli et al.*, 1999; *Margulis and Entekhabi*, 2003; *Caparrini et al.*, 2004a; *Margulis and Entekhabi*, 2004; *Ding and Wang*, 2005], the assimilation is based on the minimization of a penalty functional J with respect to the quantities to estimate over the assimilation window $[t_0, t_1]$. J contains squared errors between predictions and observations over the whole observation period and at the end of it (first and second term in equation (20) respectively), and between current and prior values of the quantities to optimize (third and fourth term in equation (20)). Here these quantities are streamflow at the beginning of the observation period and temporal evolution of the lateral inflow within it. The minimization problem is physically constrained by adjoining equation (18) to J through a vector of Lagrange multipliers $\boldsymbol{\lambda}(t) \in \mathbb{R}^n$ (last term in equation (20)).

$$
\begin{aligned}
J = & \frac{1}{t_1 - t_0}\int_{t_0}^{t_1}\left[\left(\boldsymbol{Q}(t)-\boldsymbol{Q}^{obs}(t)\right)^T\frac{\boldsymbol{K_Q}}{2}\left(\boldsymbol{Q}(t)-\boldsymbol{Q}^{obs}(t)\right)\right]dt \\
& + \left[\left(\boldsymbol{Q}(t_1)-\boldsymbol{Q}^{obs}(t_1)\right)^T\frac{\boldsymbol{K_Q}}{2}\left(\boldsymbol{Q}(t_1)-\boldsymbol{Q}^{obs}(t_1)\right)\right] \\
& + \left[\left(\boldsymbol{Q}(t_0)-\boldsymbol{Q}'(t_0)\right)^T\frac{\boldsymbol{K_{Q_0}}}{2}\left(\boldsymbol{Q}(t_0)-\boldsymbol{Q}'(t_0)\right)\right] \\
& + \frac{1}{t_1 - t_0}\int_{t_0}^{t_1}\left[\left(\boldsymbol{q_L}(t)-\boldsymbol{q_L}'(t)\right)^T\frac{\boldsymbol{K_{q_L}}}{2}\left(\boldsymbol{q_L}(t)-\boldsymbol{q_L}'(t)\right)\right]dt \\
& + \int_{t_0}^{t_1}\left[\boldsymbol{\lambda}^T(t)\left(\frac{d\boldsymbol{Q}(t)}{dt}-\boldsymbol{F}(\boldsymbol{A},\boldsymbol{Q}(t),\boldsymbol{q_L}(t))\right)\right]dt
\end{aligned}
\tag{19}
$$

The meaning of the various symbols employed in equation (20) is as follows: $\boldsymbol{Q}^{obs}(t)$ and $\boldsymbol{Q}^{obs}(t_1) \in \mathbb{R}^n$ are flow observations available at the generic time instant t and at the final instant of the assimilation window $[t_0, t_1]$, $\boldsymbol{Q}(t)$, $\boldsymbol{Q}(t_0)$ and $\boldsymbol{Q}(t_1) \in \mathbb{R}^n$ are simulated streamflows at the generic, first and final instant of the assimilation window $[t_0, t_1]$, the sign $(\cdot)'$ indicates the prior value of the quantity to estimate (in our case the initial condition for streamflow $\boldsymbol{Q}(t_0)$ and the lateral inflow at any instant inside the assimilation window $\boldsymbol{q_L}(t)$). Lastly, $\boldsymbol{K_Q}$, $\boldsymbol{K_{Q_0}}$, $\boldsymbol{K_{q_L}} \in \mathbb{R}^{n\times n}$ are weighting factors for the various error terms of J. The general idea is that the more uncertain a specific component is considered, the greater its weight is and the larger will be the correction applied to its prior value [*Margulis and Entekhabi*, 2001]. Hence, from a stochastic point of view, $\boldsymbol{K_Q}$, $\boldsymbol{K_{Q_0}}$ and $\boldsymbol{K_{q_L}}$ may be thought as related to the inverse of the covariance of their corresponding error term [*Bennett*, 1992; *Liu and Gupta*, 2007]. In practice, their relative magnitudes control the rate of convergence of the iterative procedure (described in the following) through which J will be minimized [*Castelli et al.*, 1999]. Following *Castelli et al.* [1999], $\boldsymbol{K_Q}$, $\boldsymbol{K_{Q_0}}$ and $\boldsymbol{K_{q_L}}$ are here treated simply as factors driving algorithm efficiency, since no detailed information is available on the statistical structure of the error terms. The penalty functional J is minimized if its first variation δJ vanishes. After some computations, that are reported in Appendix A, it is found that this condition is met if the following equations are satisfied:

$$
\frac{d\boldsymbol{\lambda}(t)}{dt} = \frac{\boldsymbol{K_Q}^T\left(\boldsymbol{Q}(t)-\boldsymbol{Q}^{obs}(t)\right)}{t_1 - t_0} - \frac{\partial \boldsymbol{F}^T(t)}{\partial \boldsymbol{Q}}\boldsymbol{\lambda}(t) \tag{20}
$$

$$
\boldsymbol{\lambda}(t_1) = -\boldsymbol{K_Q}^T\left(\boldsymbol{Q}(t_1)-\boldsymbol{Q}^{obs}(t_1)\right) \tag{21}
$$

$$
\boldsymbol{Q}(t_0) = \boldsymbol{Q}(t_0)' + \left(\boldsymbol{K_{Q_0}}^T\right)^{-1}\boldsymbol{\lambda}(t_0) \tag{22}
$$

$$
\boldsymbol{q_L}(t) = \boldsymbol{q_L}'(t) + (t_1 - t_0)\left(\boldsymbol{K_{q_L}}^T\right)^{-1}\frac{\partial \boldsymbol{F}^T(t)}{\partial \boldsymbol{q_L}}\boldsymbol{\lambda}(t) \tag{23}
$$

where $\boldsymbol{\lambda}(t_0)$ and $\boldsymbol{\lambda}(t_1)$ are the vectors of the Lagrange multipliers at the initial and final instant of the assimilation window. Equation (20) is a system of ordinary differential equations and represents the adjoint model of flow routing (equation (18)). It describes the time evolution of the Lagrange multipliers $\boldsymbol{\lambda}(t)$, that in the variational assimilation framework are called adjoint state variables. Equation (21) gives the terminal condition for $\boldsymbol{\lambda}(t)$ (i.e., its value at the final instant of the assimilation window) on the basis of the mismatch between simulated and observed streamflow at instant t_1. Starting from this known value of $\boldsymbol{\lambda}(t_1)$, the adjoint model (20) can be integrated backward in time, obtaining Lagrange multipliers $\boldsymbol{\lambda}(t)$ at any instant of the assimilation window. Equations (22) and (23) update the priors of, respectively, initial condition of rivers flow $\boldsymbol{Q}(t_0)$ and the temporal evolution of the lateral inflow $\boldsymbol{q_L}(t)$ on the basis of the just computed temporal evolution of $\boldsymbol{\lambda}(t)$. The estimate of $\boldsymbol{Q}(t_0)$ and $\boldsymbol{q_L}(t)$ is refined through an iterative procedure constituted by subsequent integrations of forward and adjoint model and corresponding updates. However, $\boldsymbol{q_L}(t)$ is a state variable of MOBIDIC model, determined by runoff formation and routing processes, as well as by groundwater dynamics. Hence, if it is updated without physical constraints, mass conservation is likely to be violated. Rigorously, MOBIDIC equations driving the formation of $\boldsymbol{q_L}(t)$ should be included in the derivation of the adjoint model. Nevertheless, it would be an unpractical solution, mainly because of the threshold processes that characterize soil moisture dynamics. We identify a more effective strategy in combining the variational approach with a parsimonious Monte Carlo technique. On the basis of the improved temporal evolution of $\boldsymbol{q_L}(t)$, estimated through the adjoint model and equation (23), we infer key variables that determine runoff

formation exploiting information contained in a pregenerated ensemble of $\boldsymbol{q_L}(t)$. As key variables controlling runoff, we selected initial condition of water content in capillary soil and the parameter f_0, that represents rainfall intermittence (see section 2). Soil moisture determines the partitioning of rainfall between infiltration and runoff, and f_0 can be considered as a parameter that corrects for uncertainties in both interpolation of rainfall data and hydraulic conductivity spatial distribution. At the beginning of the assimilation procedure, and only once, an ensemble of $\boldsymbol{q_L}(t)$ covering the length of the assimilation window is generated by running MOBIDIC with a number of couples of spatially homogeneous 'seed' maps of initial capillary water W_{c0} and f_0. In case sequential windows are employed, the temporal length of the ensemble spans from the initial instant of the first window to the final instant of the last window. Both W_{c0} and f_0 are varied such that the respective range of physical variability is fully embraced. Namely, W_{c0} goes from 0 to 1 in terms of saturation level, and f_0 from 0 to 1. The ensemble size is maintained small mainly thanks to the fact that the 'seed' maps are constrained to have only one degree of freedom in space, i.e., they are spatially constant. Furthermore, the range of variability of each quantity is covered using a reasonable variation step. For instance, in terms of capillary water, the aim is to distinguish between very dry, moderately dry, intermediate, moderately wet or very wet conditions. Accordingly, the saturation level is varied with a step of 15%. The step for f_0 is 0.05. Therefore, the size of the ensemble slightly exceeds 100 members. At each iteration of the variational procedure, the update equation (23) gives a *desired* trajectory of $\boldsymbol{q_L}(t)$ for any reach of the network. With *desired* trajectory meaning the temporal evolution of $\boldsymbol{q_L}(t)$ that minimizes the penalty functional *J*. The 'seed' map leading to realization with the minimum distance from this desired trajectory of $\boldsymbol{q_L}(t)$ is selected for any single river independently from the others, and the corresponding initial capillary water and f_0 fields are obtained as composites from different 'seed' maps. Hence, a spatially distributed estimate (aggregated at the level of river reach) which preserves mass balance is obtained for both quantities. The whole estimation process rests upon the adjoint model of the module for flow routing in the river network, which is a reach-based model (equation (18)). Thus, the spatial detail of the estimate is that of the river reach for any quantity ($Q(t_0)$, $q_L(t)$, W_{c0}, f_0), although the variables natively defined at this scale are only $Q(t_0)$ and $q_L(t)$ (see MOBIDIC description in section 2). The lateral inflow $q_L(t)$ works as link between the reach-based scale of the variational approach and the grid-based variables to estimate (W_{c0}, f_0). Namely, although their value is potentially different in any squared cell employed to discretize the basin, they are updated homogeneously over the cells contributing to a specif river reach, and the update is driven by the estimated temporal evolution (the *desired* trajectory) of $q_L(t)$ in that reach. Figure 1 illustrates the functioning of this mixed variational-Monte Carlo system for a specific assimilation window. Lastly, when interpreting the just-described approach, the fact that a vectorial description of the river network with a high spatial detail will be employed should be taken into account (see section 4).

In summary, for a specific assimilation window, the enhanced estimate of initial river flow $\boldsymbol{Q}(t_0)$, initial capillary water W_{c0} and f_0 is obtained through an iterative procedure that includes the following steps:

1. Generate an ensemble of $\boldsymbol{q_L}(t)$, that covers the extent of the assimilation window, by varying f_0 and W_{c0} over the basin.
2. Select suitable prior values for the quantities to estimate.
3. Run MOBIDIC in the assimilation window to obtain modeled streamflows $\boldsymbol{Q}(t)$.
4. Using streamflow observations $\boldsymbol{Q}^{obs}(t)$ inside the assimilation window, integrate backward in time the terminal value problem (20), (21) to obtain the adjoint state variables $\boldsymbol{\lambda}(t)$ in the assimilation window. Namely, first evaluate the terminal condition for adjoint variables through equation (21), and then, starting from the just obtained value of $\boldsymbol{\lambda}(t_1)$, integrate backward in time the system of ordinary differential equations (20) up to the first instant of the assimilation window t_0.
5. On the basis of the just obtained values of $\boldsymbol{\lambda}(t)$, update the prior estimate of $\boldsymbol{Q}(t_0)$ and $\boldsymbol{q_L}(t)$ through equations (22) and (23) respectively.
6. Select, for each river reach independently, the realization of the ensemble that minimizes the distance from the just updated temporal evolution of $\boldsymbol{q_L}(t)$. Associate the corresponding W_{c0} and f_0 to the contributing cells, such that spatially distributed maps (river reach spatial scale) of W_{c0} and f_0 are obtained.
7. Adopt updated $\boldsymbol{Q}_0$, W_{c0} and f_0.
8. Restart from step 3 until some convergence criterion is met.

The adjoint model is composed by a set of ordinary differential equations that are coupled on the basis of network topology. This implies that the procedure is not limited to reaches for which observations are

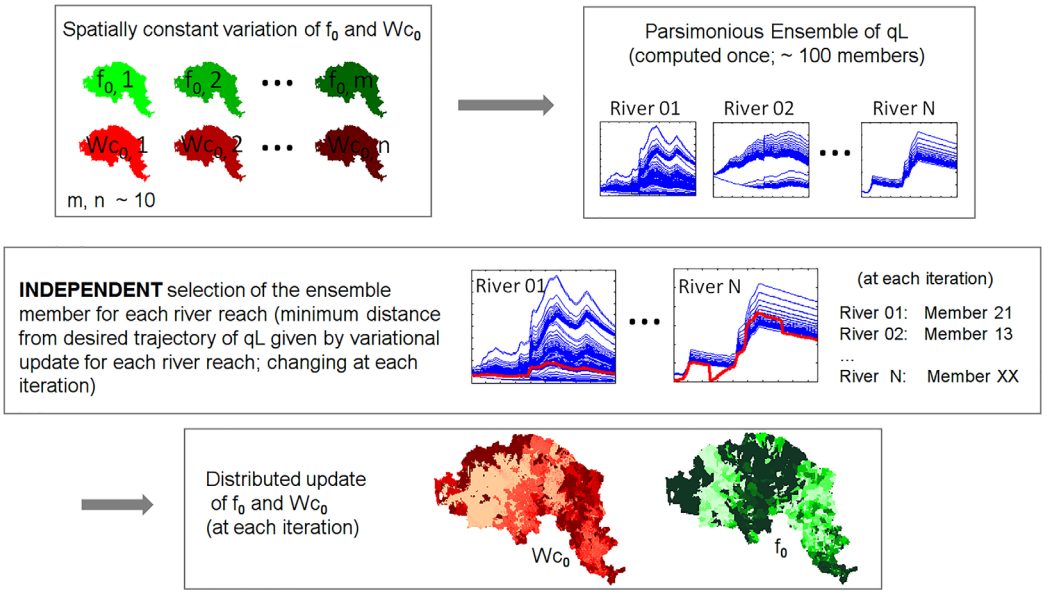

Figure 1. Scheme of the mixed variational-Monte Carlo assimilation system.

available, but corrections spread upstream. The advantage is that all the river network could potentially benefit from the data assimilation, improving model performances even in ungauged reaches. However, the coupling poses also potential issues, since the adjoint model may have to deal with discordant forcings from downstream. For instance, observations may be greater than the modeled flow in a certain location and lower in another, both trying to spread their opposite tendency to the same upstream part of the network.

4. Hindcast Experiments

The performances of the assimilation system are assessed through several hindcast experiments in Arno river basin, central Italy. The variety of the considered events allows an overall evaluation of the actual improvement that it can lead to flood forecasting operations. A flood forecasting chain benefits not only from more accurate predictions during high flow events, but also from a reduced number of significant overestimations of streamflow that may cause false alarms. Accordingly, a real-time oriented evaluation of the assimilation system should verify its effectiveness in both situations, i.e., the selection of case-study events should be based not only on river hydrographs but also on rainfall accumulation. This will bring in the analysis also those cases where intense rainfall did not produce significant flood waves. Details about the area of study and the hindcast experiments are given in sections 4.1 and 4.2 respectively.

4.1. Area of Study and Data

Arno river basin extends over about 8300 km^2 and is bounded by the Appennine mountain range from north to east. Average and maximum elevation are about 350 and 1600 m a.s.l. respectively. Arno is the main river of Tuscany region, and its mainstream is about 240 km length. Flood forecasting is a relevant concern in Arno basin, since Arno passes through major Tuscan cities, as Florence and Pisa. Climatic conditions are semiarid with large seasonality and a mean annual precipitation of nearly 800 mm. The population living in the basin is about 22,00,000, corresponding to the high average density of 265 people/km^2. However, the population is mainly concentrated in cities, whose spatial extent covers a small portion of the basin. The urban area to consider impervious from a hydrologic modeling point of view corresponds to about 5%, while the main land cover types are cropland, olive-yards, vineyards and forest. Three reservoirs are present in the basin. Two are dedicated to energy production, with no floods control at the current stage. The third one is for water supply. It is placed in the initial part of a tributary which flows into Arno

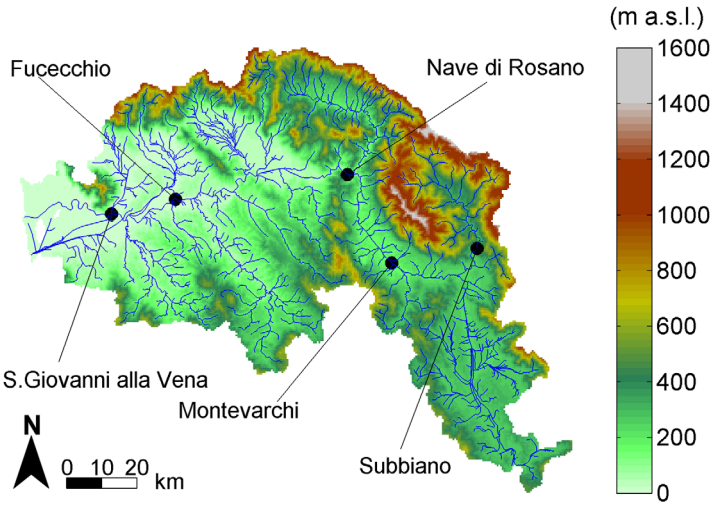

Figure 2. Digital Elevation Model (DEM) and river network of Arno basin used in the simulations. Black circles indicate the available flow measurement stations. DEM is plotted at the resolution employed in the simulations, i.e., 500 m.

river upstream the city of Florence. It drains an area equal to about 4% of the total contributing to the mainstream in correspondence of the confluence, and to less than 2% of the total watershed.

Figure 2 shows Digital Elevation Model, river network and the location of flow measurement stations employed in this work. They are all located along Arno river, with S. Giovanni alla Vena station being the closest to basin outlet. On the basis of rainfall and discharge data from some selected events among those examined in this study, watershed response time at S. Giovanni alla Vena is estimated to be in the range 17−25 h, mainly around 20 h. As frequently done, the centroid-lag-to-peak, i.e., the time between the centroid of the hyetograph and the flow peak, is employed for the estimates [*Dingman*, 2008]. To complete the presentation of the 5 gauge stations, the centroid-lag-to-peak of each one is shown in Figure 10 for one of the examined events. All the stations provide streamflow data every 15 min. Furthermore, in the area of interest, 102 thermometers, 70 hygrometers, 165 pluviometers, 50 anemometers and 31 radiometers are available for the study, with data at the temporal resolution of 15 min. They are all located inside the basin, or in proximity of it, distributed almost homogeneously over the area. To force the model, data from all the available measurement sites are interpolated through Inverse Distance Weighting, obtaining maps of micrometeorological quantities at the appropriate spatial resolution (i.e., the spatial resolution employed to run the model, that is specified in the next section). Different power parameters are used to interpolate the various quantities, and a correction for elevation is applied exclusively in case of air temperature. Rainfall is the main micrometeorological forcing relevant to this study, since we are conducting an event-based evaluation. Precipitation data are interpolated with the power parameter equal to 6, meaning that the weight of the closest pluviometer is rapidly predominant over the others. The 3 reservoirs present in the basin are not included in the simulations, since in the current management setup they are not assigned to relevant flood regulation operations. As described in the first paragraph of the present section, the two hydroelectric reservoirs are not effective for floods control, while the third one may impact only slightly on flood waves also at the closest measurement station (Nave di Rosano). The area drained by the reservoir is small (about 4%) in respect to that contributing to the flow at this location.

As presented in section 2, the main parameters driving soil hydrologic behavior in MOBIDIC are the hydraulic conductivity, K_s, and the maximum storage capacity of soil gravitational(capillary) compartment, $W_{g,\max}$ ($W_{c,\max}$). Following the current operational setup of MOBIDIC at the hydrologic service of Tuscany region, the values here adopted for these parameters are those officially provided by Tuscany region through a map including hydrologic characterization of soil for the whole regional territory. For details about the methods and the database employed to derive such map, we refer to the associated technical documentation [*Gardin*, 2014], while here we briefly summarize only the rationale. Both hydraulic conductivity and soil water content at various potentials (from which $W_{g,\max}$ and $W_{c,\max}$ can be computed directly) have been estimated through pedo-transfer functions applied to a large database of soil horizons (about 13,800, corresponding to 3800 vertical profiles). The employed pedo-transfer functions have been selected from those available in the literature on the basis of admissibility tests and validation against measured values. Different pedo-transfer functions have been selected for different soil texture classes. The hydraulic conductivity has been corrected to the take into account the presence of rock fragments, and its minimum value in the first 30 cm of soil has been assumed to be representative of infiltration processes. The thickness of the soil

Table 1. Mean Total Precipitation Over the Basin, P (mm), Observed Peak Flow, Q_{max} (m^3s^{-1}), Percentage Error on the Peak Flow, PE (%), Timing Error of the Flow Peak, E_{time} (hours), Logarithmic Nash-Sutcliffe Efficiency, η, and Root Mean Square Error, RMSE (m^3s^{-1}), in Open Loop Simulations at the Available Measurement Stations for High Flow (From E_{01} to E_{10}) and False Alarm (From E_{11} to E_{16}) Events (n.a. Means That Observations are Not Available)

	E_{01}	E_{02}	E_{03}	E_{04}	E_{05}	E_{06}	E_{07}	E_{08}	E_{09}	E_{10}	E_{11}	E_{12}	E_{13}	E_{14}	E_{15}	E_{16}
P - MEAN	65	42	47	68	87	70	45	58	68	90	41	74	36	44	37	49
Q_{max}- SUBB	512	576	591	448	198	347	577	436	448	490	147	55	82	116	1	8
Q_{max}- MONT	840	544	902	684	506	389	1069	852	1080	471	251	88	75	140	2	61
Q_{max}- NAVE	1162	910	1657	851	739	568	1281	959	1097	622	430	202	220	278	31	83
Q_{max}- FUCC	1979	n.a.	1983	1491	1443	n.a.	1409	n.a.	1088	980	676	361	346	247	118	104
Q_{max}- SGIOV	1932	1929	1924	1820	1730	1534	1507	1497	1077	990	715	398	369	215	125	109
PE - SUBB	−38.0	−40.0	−29.5	−73.8	−1.1	−53.8	−11.9	−0.7	−27.1	−73.6	54.9	210.5	47.7	207.2	>999	>999
PE - MONT	−48.4	−16.8	−24.9	−55.4	−37.0	−38.0	−29.2	20.3	−25.3	−58.6	43.0	164.1	194.7	209.8	>999	362.2
PE - NAVE	−39.6	−10.8	−23.7	−40.2	−34.0	−33.4	−18.0	35.5	−19.9	−44.4	50.1	99.4	65.7	115.8	>999	539.3
PE - FUCC	−25.7	n.a.	−5.2	−41.6	−40.6	n.a.	−3.3	n.a.	−14.2	−46.9	42.4	125.7	68.7	206.0	558.0	682.9
PE - SGIOV	−15.5	−25.9	−4.0	−44.7	−41.8	−35.1	−3.5	8.4	−8.7	−40.5	43.3	151.9	75.1	269.2	641.4	814.8
E_{time}- SUBB	0.00	0.00	−0.50	−0.25	0.25	2.75	−0.50	−0.50	0.00	−0.75	−0.75	−2.75	−2.25	0.00	−34.75	−5.50
E_{time}- MONT	−1.00	0.00	−0.75	−0.50	−1.75	1.50	0.00	−0.25	0.25	−1.00	−3.00	−1.50	−9.50	3.75	3.75	0.00
E_{time}- NAVE	−1.50	−1.50	−1.25	−2.00	0.50	−0.50	−2.50	−3.50	−1.25	−2.50	−4.50	−2.25	2.75	3.25	−3.75	−4.50
E_{time}- FUCC	−1.25	n.a.	−0.25	−5.50	−0.75	n.a.	−1.25	n.a.	1.00	1.00	−2.25	−2.00	0.25	3.25	1.50	4.00
E_{time}- SGIOV	2.50	−2.00	−0.50	−8.50	−2.50	−3.75	−1.75	−0.50	1.50	0.75	1.75	−1.00	1.50	4.25	−1.75	3.50
η - SUBB	1.59	1.16	2.26	0.19	1.48	0.76	2.63	1.33	1.92	0.15	−0.22	−3.12	−0.03	−2.79	−11.21	−6.57
η - MONT	0.50	1.54	2.42	0.40	0.49	0.15	2.15	0.76	1.85	0.22	−0.39	−2.78	−2.07	−3.35	−13.39	−3.51
η - NAVE	0.49	1.88	1.72	0.39	−0.44	−0.25	2.46	0.17	1.97	0.09	0.27	−2.48	−0.45	−2.19	−6.45	−4.43
η - FUCC	1.02	n.a.	1.58	0.58	−0.79	n.a.	2.84	n.a.	2.26	0.23	0.72	−3.62	−1.16	−2.80	−4.71	−4.91
η - SGIOV	1.33	0.94	1.89	0.66	−0.26	0.86	2.45	0.34	1.84	0.37	0.56	−3.87	−1.45	−3.35	−5.07	−5.52
RMSE-SUBB	52	79	47	94	20	50	43	54	41	87	35	51	19	83	21	39
RMSE-MONT	147	54	60	144	80	95	102	131	117	90	69	107	63	131	74	93
RMSE-NAVE	239	72	175	183	168	160	101	202	113	153	89	129	74	165	173	189
RMSE-FUCC	331	n.a.	236	325	363	n.a.	98	n.a.	105	255	130	310	143	271	350	337
RMSE-SGIOV	293	274	204	396	349	280	121	315	118	221	148	425	179	307	465	440

contributing to $W_{g,max}$ and $W_{c,max}$ has been assumed to be the minimum between 1.5 m and the depth at which the first rock layer is encountered. Results are spatialized using pedologic criteria based on soil typological units and soil-landscape relationships.

4.2. Experiments Setup

In order to evaluate the gain in flood forecasting that can be obtained through the assimilation system, 16 hindcast experiments are performed. They include both high flow and false alarm events (high rainfall but low flow) that occurred in the period 2009−2014. Table 1 lists, for all the examined events, observed values of flow peak at the available measurement stations (Q_{max}) and mean total precipitation over the basin (P). The events are named in descending order of observed peak flow at S. Giovanni alla Vena station, i.e., E_{01} has the maximum peak flow and E_{16} the minimum one. Furthermore, in Figure 3, the peak flow at S. Giovanni alla Vena station is plotted in function of the mean total precipitation in the drainage basin for each examined event. The almost complete absence of correlation between P and Q_{max} shows that a proper hydrologic modeling is fundamental for a correct flood forecasting.

Simulations are run with spatial and temporal resolutions that are employed operationally at the hydrologic service of Tuscany region, i.e., 500 m and 15 min. Comparing the size of the square grid (0.25 km^2) with the extension of the basin (about 8300 km^2), it can be asserted that we are running high resolution simulations. Also the vectorial description of the river network is spatially detailed, with an average extent of the contributing area for each river reach equal to 7.1 km^2. The values adopted for MOBIDIC conceptual parameters (α=8.5e-06 s^{-1}, β=7.62e-06 s^{-1}, k=1.4e-05 s^{-1}, γ=1.68e-08 s^{-1}) have been identified through a *trial-and-error* new calibration over 5 relevant events in the period 2010–2014, obtaining average (over events) Nash-Sutcliffe efficiencies of 0.51, 0.67, 0.66, 0.78 and 0.73 at Subbiano, Montevarchi, Nave di Rosano, Fucecchio and S. Giovanni alla Vena stations. None of these calibration events is included in the evaluation of the assimilation system. The calibration on the 2010–2014 events updates a set of first guess values previously used to run the model over the same watershed [*Campo et al*., 2006; *Castelli et al*., 2009].

Data from the five measurement stations are employed simultaneously in the assimilation. The procedure (with mixed variational-Monte Carlo approach) described in section 3 is applied sequentially on not

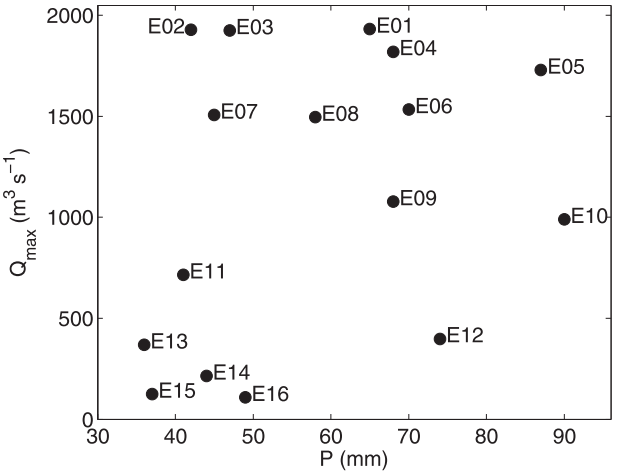

Figure 3. Maximum observed streamflow, Q_{max} ($m^3 s^{-1}$), at S. Giovanni alla Vena station in function of the mean total precipitation in the drainage basin, P (mm).

overlapping windows of 6 h. Repeating in sequence the assimilation every 6 h is judged a valuable strategy to use the developed system for operational flood forecasting, as it allows predictions to be corrected since the early stage of the event. Employing a longer assimilation window would spread the correction due to any local mismatch between observations and predictions farther upstream, affecting a broader portion of the watershed. The upstream diffusion of the update is due to the coupling between the differential equations composing the adjoint model of the river network routing module (see section 3.1). In presence of various points of assimilation, a window much longer than the travel time between them leads to force adjoint equations of upstream reaches on the basis of multiple downstream observations. In some cases, an excessive superposition of forcings may weaken the impact of the assimilation, e.g., if model-data mismatches are discordant at the various locations. A window of 6 h, combined with the spatial distribution of the 5 assimilation locations here employed, updates the majority of the basin without causing an undue combination of forcings. The blocks of 6 h are predetermined over the hours of a day, i.e., the first block in 1 day is always 0−6, the second one 6−12, the third one 12−18 and the last one 18−24. The reason is again to facilitate the operational usage of the system. For each event, the first assimilation window is the block of the day containing, or the time at which rainfall starts, or the instant at which streamflow begins to rise. The condition to apply is decided in function of the specific event. Analysis of initial discharge in the river network and capillary water in soil, as well as the optimal estimate of the parameter f_0, are obtained for each assimilation window, and then used to run the corresponding prediction simulation. Usually, the mismatch between simulated and observed discharge at a certain instant is directly converted into an update for soil moisture. In this case, the update should be applied with a lag time that is appropriate for the location at which it is assigned (i.e., to effectively reduce the streamflow mismatch at the instant it is detected, flow travel time between the point of the watershed where soil moisture is corrected and the point where streamflow is observed must be considered). In the assimilation system we present, as comprehensively described in section 3.1, initial soil water content is not directly updated through the variational approach, i.e., it does not compute the increment for W_c. The variational part provides the time evolution of the lateral inflow that should enter each river reach during the observation period to reduce streamflow mismatch between model and measures. This time evolution is used as a finger print to 'pick up' a model realization from a pregenerated ensemble that covers all the possible range of evolution determined by treating W_c (and f_0) as unknown. Thus, time lag is implicitly taken into account through this step. As the assimilation window advances in time (i.e., more time passes since rainfall started), an increasing portion of the watershed can be updated correctly. The lead time associated with each prediction run is computed as the difference between the time of observed peak flow and the final instant of the corresponding assimilation window. Accordingly, a negative lead time indicates that the assimilation window includes the observed peak. The weighting matrices of the penalty functional to minimize (equation (20)) are taken diagonal, i.e., errors are assumed to be statistically independent following *Seo et al.* [2003, 2009] and *Lee et al.* [2011, 2012]. For each event, the quantitative evaluations that are described and discussed in the next section are conducted over the hydrograph comprised between the first instant of the first assimilation window and the instant of the falling limb at which streamflow comes back to the order of magnitude of the beginning.

In addition to the just described experiments, other 16 assimilation tests are performed. They are identical under every aspect to the first 16, except that streamflow observations are not assimilated at S. Giovanni alla Vena station. The goal of these second group of experiments is to give a very first insight into the capabilities of the assimilation system at ungauged locations. A more elaborate investigation would be needed

for a comprehensive assessment of system performances at ungauged points, but this goes beyond the aim of the present work. S. Giovanni alla Vena station has been selected as test site because, from an operational perspective, the main interest is in improving predictions at downstream locations through upstream assimilation.

5. Results

Flow predictions accuracy is evaluated in terms of error on flow peak and Nash-Sutcliffe efficiency, here employed in a logarithmic form (η) that is part of a likelihood function examined in *Cheng et al*. [2014]:

$$\eta = -\ln(1-\mathrm{NSE}) \tag{24}$$

with Nash-Sutcliffe efficiency (NSE) computed as:

$$\mathrm{NSE} = 1 - \frac{\sum_{i=1}^{N}\left(Q_i^{mod} - Q_i^{obs}\right)^2}{\sum_{i=1}^{N}\left(Q_i^{obs} - \overline{Q^{obs}}\right)^2} \tag{25}$$

where Q_i^{obs} and Q_i^{mod} are observed and modeled flow values, N is their total number, and the overbar means averaging. To readily interpret values of η, consider that it preserves the sign of NSE and its range is $(-\infty, +\infty)$, namely it tends to plus infinity in case of perfect match between model and observations (NSE=1). Moreover, a value of NSE equal to 0.9 corresponds to η=2.3. The main reason to use the logarithmic NSE is that in our set comprising events of different nature (with both high and extremely low flows) and highly variable model performances (as it will be discussed in the following), NSE spans a broad range. In fact, in false alarms it is likely to obtain a NSE significantly lower than zero (it is the result of low and flat observed flows combined with rather high predicted values). The adoption of a logarithmic scale allows to better deal with largely negative and high values (close to 1) of NSE at the same time. Namely, we exploit the fact that η stretches the NSE range $(-\infty, +1)$ over $(-\infty, +\infty)$. In addition to logarithmic NSE, also the Root Mean Square Error (RMSE) is employed to measure global performances of each run:

$$\mathrm{RMSE} = \sqrt{\frac{\sum_{i=1}^{N}\left(Q_i^{mod} - Q_i^{obs}\right)^2}{N}} \tag{26}$$

where notation is maintained coherent with that employed in the definition of NSE.

Values of the percentage error (PE) on peak flow, the corresponding timing error, η and RMSE are reported in Table 1 for Open Loop (OL) runs, i.e., without data assimilation. OL simulations are started about 15 days before the examined events and run continuously till after the end of each event. For false alarm events (from E_{11} to E_{16}), note that, in addition to negative η, also high percentage errors are present because of the extremely low values of observed streamflow (e.g., percentage errors greater than 999% at Subbiano, Montevarchi and Nave di Rosano for event E_{15} correspond to 1, 2 and 31 m^3s^{-1} of observed peak). These events are characterized by hydrographs with flows of few m^3s^{-1} or lower, in some cases almost flat, although a rather relevant precipitation occurred. A comparable rainfall with comparable rainfall accumulation in the antecedent two weeks may generate a noticeable runoff in other occasions, and reproducing such wide variability of responses is challenging for mathematical models when parameters are fixed. Namely, models structures (equations used to describe complex interconnected phenomena) are usually too rigid in respect to reality. Table 1 shows that, besides the variability in the kind of events (i.e., both high flow and false alarms events), we are considering also a wide range of model performances. Open loop simulations provide both poor (e.g., E_{10}, E_{12}) and good (e.g., E_{07}, E_{09}) agreement with observations, as well as intermediate situations (e.g., E_{02}, E_{04}).

Figure 4 provides an overall evaluation of the assimilation system performances. It reports the difference between the logarithmic Nash-Sutcliffe efficiency in data assimilation simulations, η, and its corresponding value in open loop runs, η_{OL}, in function of lead time (panels a-e). The increments are plotted in separate panels for each measurement station, and a different symbol is used for any examined event. In particular, black symbols are for events whose observed peak flow at S. Giovanni alla Vena station is greater than 1600 m^3s^{-1}, gray symbols are for the range 500−1600 m^3s^{-1}, and white symbols are for peak flows lower

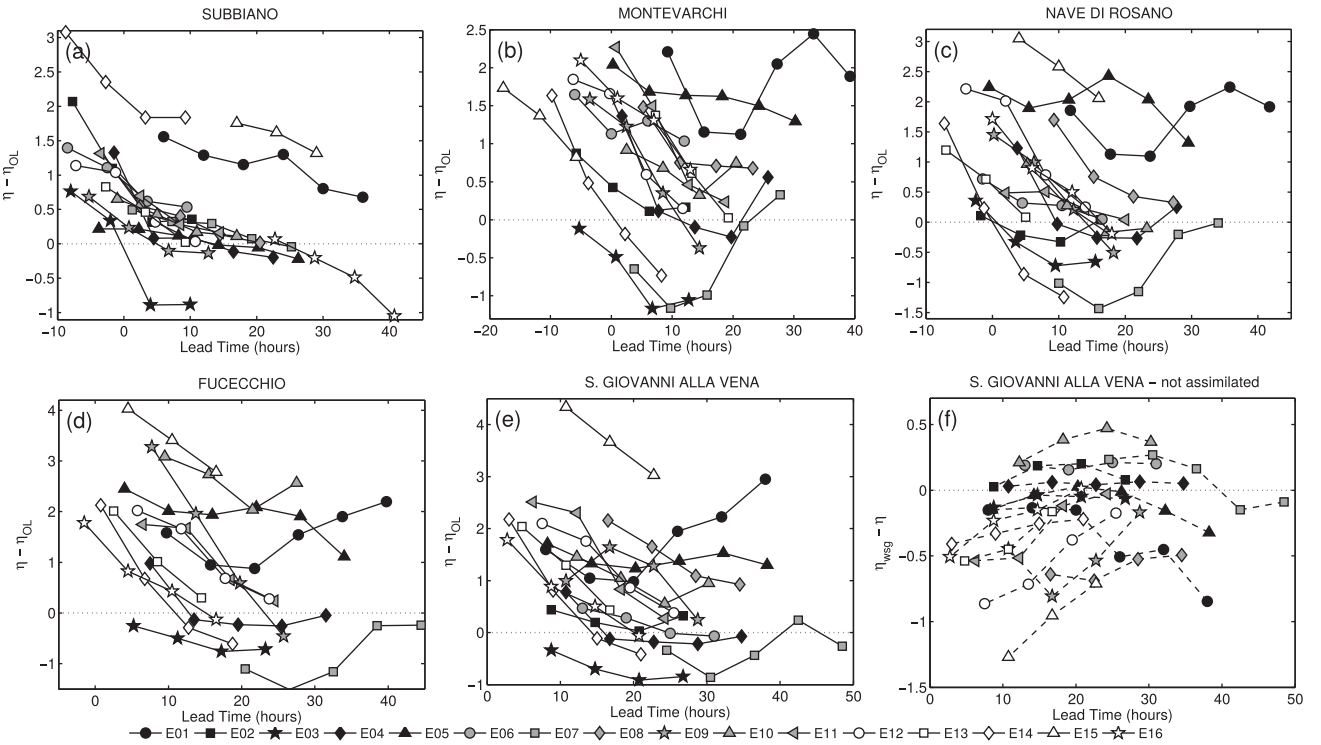

Figure 4. (a–e) Difference between logarithmic Nash-Sutcliffe Efficiency in data assimilation simulations (η) and the corresponding open loop value (η_{OL}) in function of lead time for all the analyzed events at the available measurement stations. (f) Difference between logarithmic Nash-Sutcliffe Efficiency in simulations that do not assimilate streamflow data at S. Giovanni alla Vena (η_{wsg}) and the corresponding value in simulations that do assimilate at S. Giovanni alla Vena.

than 500 m^3s^{-1}. In the plots, a positive value indicates an enhancement of predictions in respect to open loop. Remember that a unique lead time is associated to each run in its entirety, defining it as the difference between the time of locally observed peak flow and the final instant of the corresponding assimilation window. The general behavior at all the locations is, as desired, an increase of η as lead time reduces, and an improvement in respect to open loop. The enhancement occurs for both high flow and false alarm events. Although the level of the gain is variable among the various events and locations, in numerous cases η increases of 0.5 or more in respect to open loop with a lead time of about 10 h, that is comparable with the response time of the basin at the various stations (see Figure 10 for an estimate of response times in one specific event). Hence, results show that the assimilation system can significantly improve the prediction of flow time evolution. Results reveal also some differences between the examined locations. First, at downstream stations (Fucecchio and S. Giovanni alla Vena) the increment of η is generally greater. Such behavior is probably due to the fact that downstream sites benefit not only from the local assimilation, but also from that at multiple upstream points. Second, the spread of the increment obtained at a fixed lead time between the various events is small at Subbiano, while it is remarkable at all the other locations. This indicates that, as the complexity of the upstream river network and the amount of the employed information increase, the assimilation system becomes more flexible, being more dependent on the characteristics of the specific event. At the same time, the fact that flexibility enlarges while moving downstream makes the system more prone to produce greater improvements at Fucecchio and S. Giovanni alla Vena stations. Exceptions to the diffuse positive impact of the data assimilation scheme on model results are high flow events E_{07} and E_{03} (marked with gray squares and black stars respectively), and, to a lesser extent, the false alarm E_{14} (marked with white diamond symbols). In both E_{07} and E_{03} the open loop run already generates accurate predictions at all the stations, with an average η of 2.51 and 1.97 respectively (see Table 1). The assimilation system cannot further enhance these already good performances, and causes a worsening of the overall accuracy of predictions, especially in the first assimilation windows. This suggests that, in presence of a good match between simulation and observations, an additional forcing of modeled flows toward observed flows could be deleterious. Further insight into this aspect will be given in the following, when

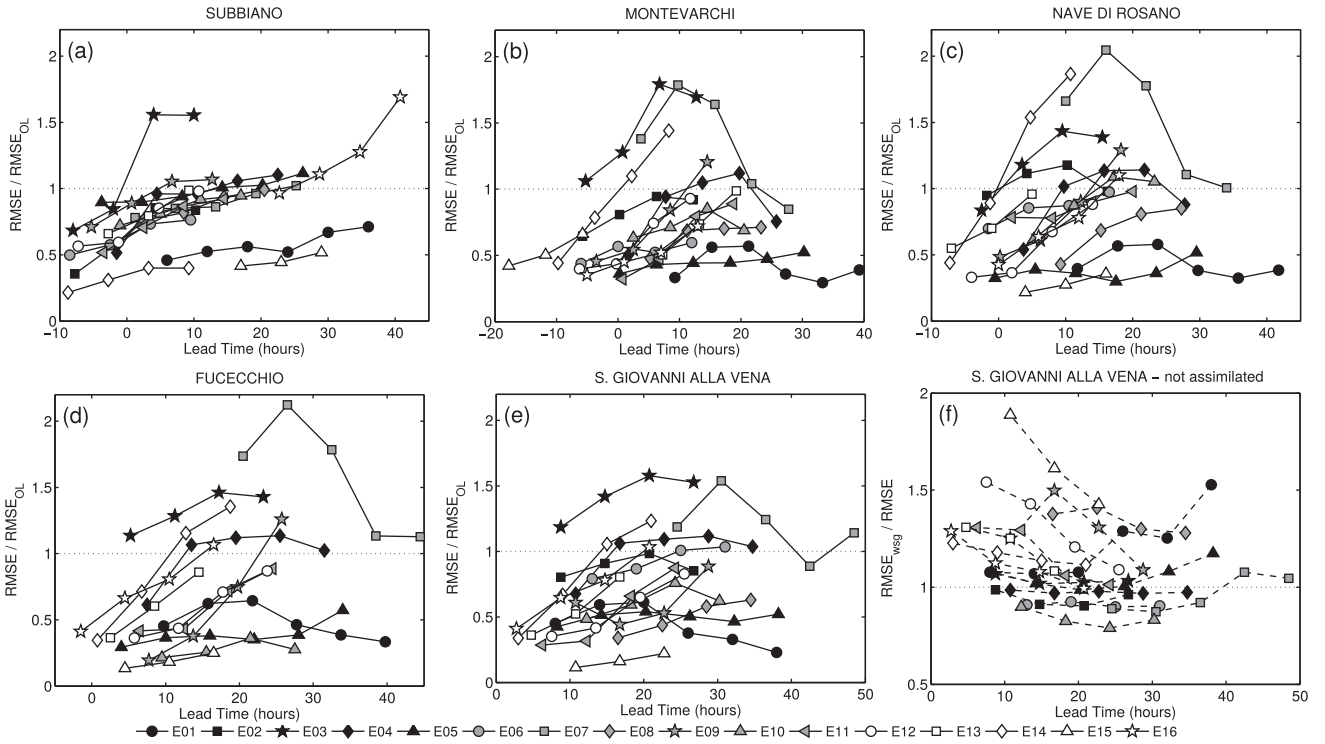

Figure 5. (a-e) Root Mean Square Error in data assimilation simulations (RMSE) and the corresponding open loop value ($RMSE_{OL}$) in function of lead time for all the analyzed events at the available measurement stations. (f) RMSE in simulations that do not assimilate streamflow data at S. Giovanni alla Vena ($RMSE_{wsg}$) normalized with respect to the corresponding value in simulations that do assimilate at S. Giovanni alla Vena.

the hydrographs of event E_{07} will be analyzed. However, continuing with the assimilation, η re-start to increase, with the tendency of recovering the accuracy of the open loop as lead time reduces. In E_{03}, η of the last assimilation run nearly equals, or surpasses, that of the open loop at the various locations. The evolution of η in function of lead time suggests an analogous behavior for E_{07}, although the assimilation sequence is stopped before that performances of open loop could be recovered. This fact, i.e., that the assimilation scheme can remedy its possible malfunction, indicates its robustness. Anyway, note that the values of η remain quite high for both events at all the locations despite the worsening. Hence, in its worst performances, the assimilation system does not cause a dramatic drop of predictions accuracy. Regarding false alarm E_{14}, the explanation for the initial worsening of results is different. Open loop run dramatically overestimates stream flow at all the locations, as shown by the relative errors on the peak reported in Table 1. However, during the period corresponding to the first two assimilation windows, simulated and observed streamflows are almost in accordance, being both of the order of few m^3s^{-1} at all the stations. Hence, the assimilation scheme receives an ambiguous information, coming from a weak signal, and cannot update properly model states and parameters on its basis. As soon as observed and simulated streamflows start to diverge (since the third window), the system acts correctly and predictions accuracy improves, with an increment of η of 0.5 or more at all the locations.

The previous considerations conform also to Figures 5a–5e, which shows the RMSE of each prediction run normalized with the RMSE of the open loop simulation and plotted in function of the corresponding lead time. Values lower than 1 indicate improved predictions in respect to open loop. Overall and specific (in terms of both event and location) behaviors noticed in Figure 4 are present also in these plots, verifying that the use of η to assess runs performances is reasonable. Here, a lead time of about 10 h corresponds frequently to a reduction of the RMSE of nearly one half (except that at Subbiano, where the diminution for the same lead time is mainly around 15%). In several cases, at Fucecchio, S. Giovanni alla Vena and Nave di Rosano, the reduction reaches 70%.

Since accurately forecasting flow peak is one of the most important skills for flood early warning, a specific evaluation of the gain that the assimilation scheme can provide on it is performed. Figure 6 reports, for

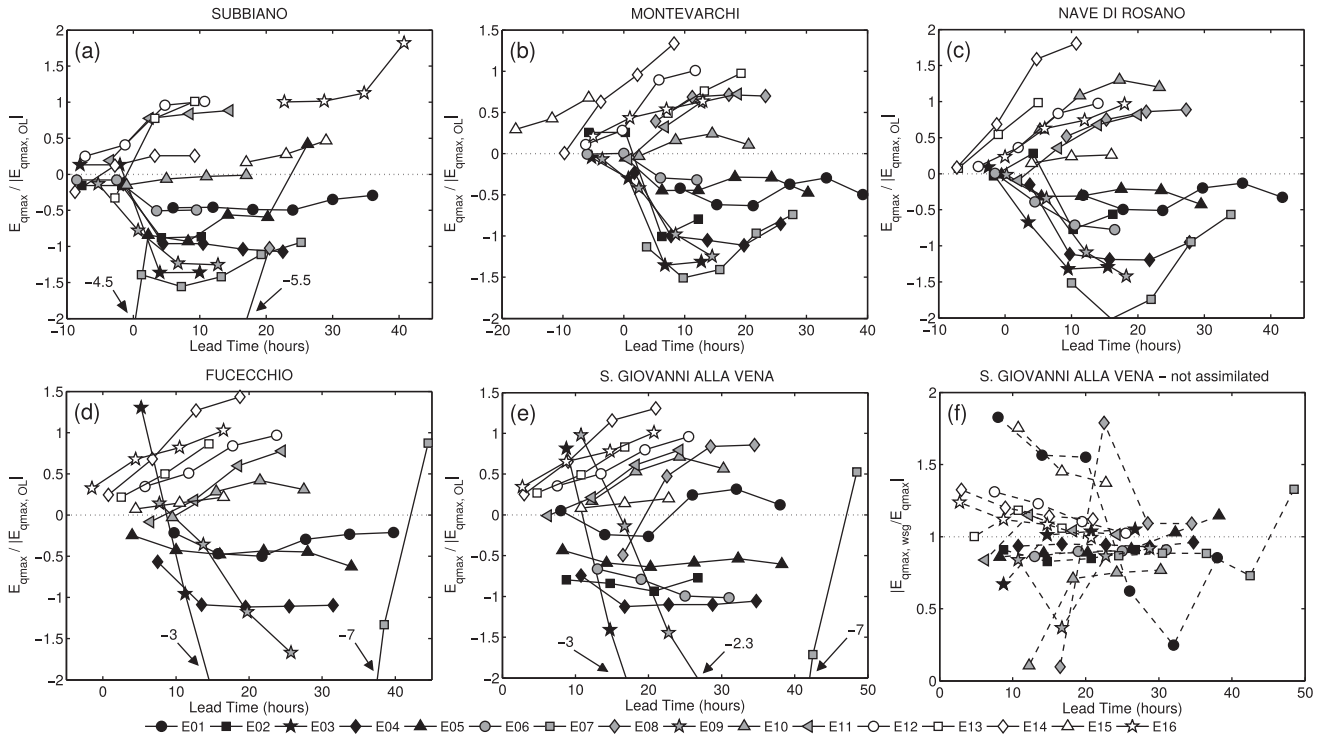

Figure 6. (a-e) Flow peak error in data assimilation simulations normalized with respect to the corresponding open loop error (absolute value) in function of lead time for all the analyzed events at the available measurement stations. (f) Flow peak error in simulations that do not assimilate streamflow data at S. Giovanni alla Vena ($E_{qmax,wsg}$) normalized with respect to the corresponding value in simulations that do assimilate at S. Giovanni alla Vena.

each measurement station, the error on peak flow normalized with the corresponding value in open loop simulation (absolute value) in function of lead time (panels a-e). In general, the error is smaller than that of the open loop, and decreases as lead time reduces. Relevant improvements are reached at each station, with a gain of more than 50% in respect to open loop for numerous experiments with a lead time of around 10 h. In particular, peak flow forecasts at S.Giovanni alla Vena and Fucecchio significantly enhance when flow peak in the upstream locations is included in the assimilation window (i.e., for negative lead times at Subbiano, Montevarchi and Nave di Rosano). However, specific performances are highly event-dependent and data assimilation can also worsen peak forecasting. For instance, this is the case of flood events E_{09}, E_{07} and E_{03} (marked with gray stars, gray squares and black stars in Figure 6). Data assimilation initially increases flow peak error in respect to open loop at any station. As the assimilation window advances in time, improvements are obtained upstream, while downstream they are not achieved. The reason for this behavior is twofold. First, these events are all characterized by an open loop with a low percentage error in peak flow at the various measurement stations, and especially at those located downstream (see Table 1). The values for S. Giovanni alla Vena are −8.7%, −3.5% and −4.0% respectively. Therefore, in presence of already accurate predictions, it is arduous to provide additional enhancement. Moreover, a slight worsening corresponds to significant values in the plot because of the normalization by a small open loop error. Second, observations at the various locations are not always fully coherent between them, since measurement errors are also present, especially in presence of high flows. Hence, upstream corrections may be discordant with downstream data, and cause a slight deterioration of already accurate predictions.

Figure 7a offers an aggregated view of the just-discussed results. It shows boxplots of normalized peak error from all the stations and hindcast experiments, subdividing results into 5 ranges of lead time, namely lead time grater than 24 h, between 24 and 12, 12 and 6, 6 and 0 and lower than 0. The third class is that containing lead times comparable with basin response time at all the examined locations (see Figure 10 for response times). The median of the normalized error is smaller than 1 for all the 5 classes, meaning that open loop predictions are likely to be enhanced by data assimilation even with a relevant advance. However, the impact of the assimilation system is characterized by a quite large variability until lead time is greater

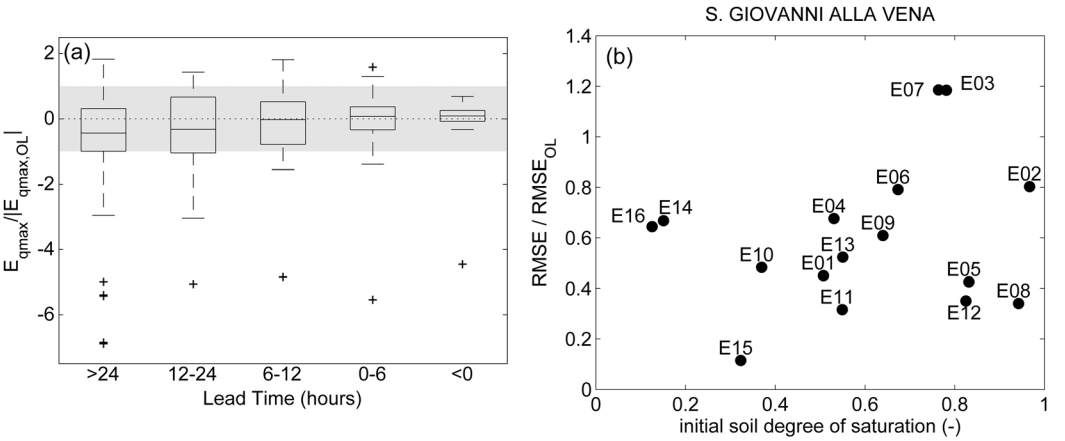

Figure 7. (a) Boxplots of normalized flow peak error for all the measurement stations and analyzed events. Normalization is with respect to the corresponding value in open loop simulations. The gray band highlights the range $(-1; +1)$, i.e., where error from data assimilation runs is reduced in respect to OL. (b) Reduction of RMSE in respect to OL at S. Giovanni alla Vena station with a lead time of about 10 h as a function of the average soil saturation at the beginning of the assimilation.

than 12 h, with a 25th percentile of nearly 1 in both first and second class. As lead time decreases, the median of normalized peak error approaches zero and the variability in performances reduces. Hence, the effectiveness of the assimilation system enhances and becomes increasingly event-independent with shorter forecast horizons.

To give further insight into the gain obtainable with the assimilation system, hydrographs for 4 of the 16 examined events are shown in Figures 8–11. They correspond, respectively, to the false alarm event E_{11} and to high flow events E_{09}, E_{10} and E_{07}. Observations are gray dots, with those used in the assimilation marked with diamond symbols. Open loop simulation is the solid line, predictions from assimilation of flow data during the first, second, third, and fourth and assimilation window are the dotted, dashed, dash-dot and

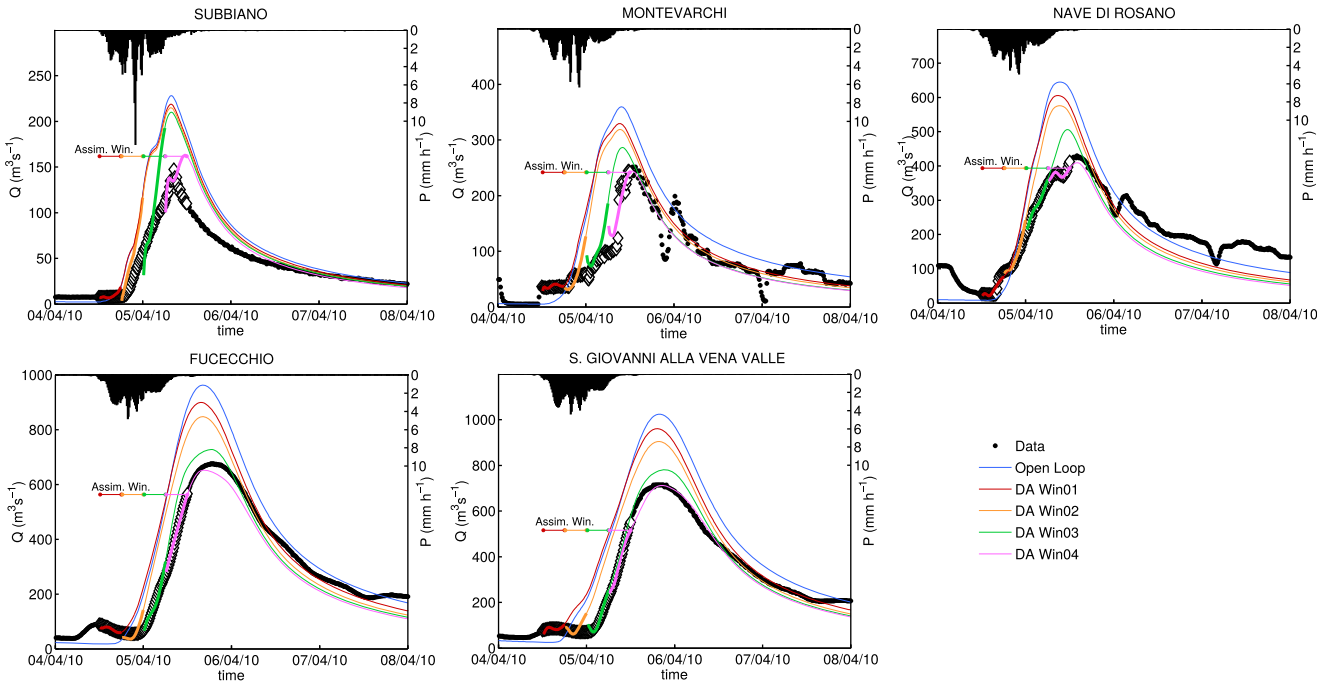

Figure 8. Hydrographs at the measurement stations for the false alarm event E_{11}. Flow observations are gray dots, with those used in the assimilation marked with diamond symbols. Open loop simulation is the solid line, predictions from the assimilation of flow data during the first, second, third, and fourth assimilation window are the dotted, dashed, dash-dot and solid thick line respectively. Mean precipitation intensity in the drainage basin is reported in the second axis of the plot.

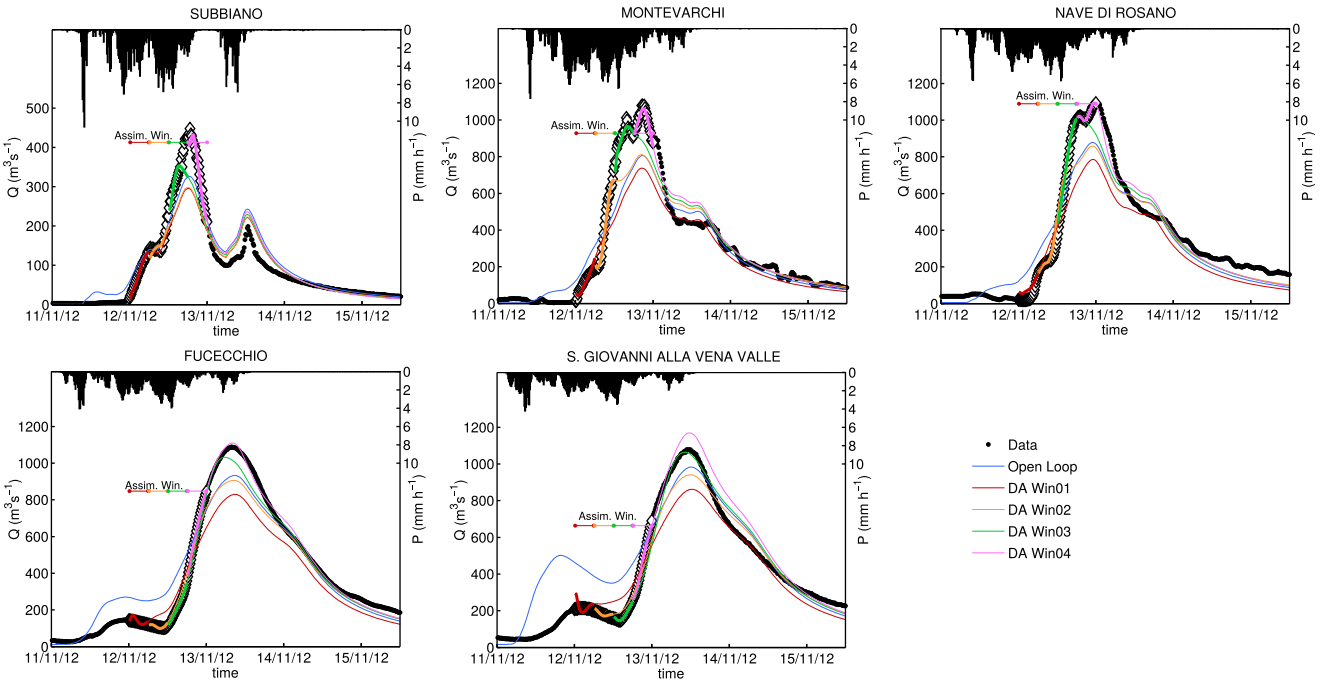

Figure 9. As in Figure 8 but for the high flow event E_{09}.

solid thick line respectively. The 4 experiments show different impacts of the assimilation system on predictions. In event E_{11}, the overestimation of the open loop is progressively corrected by data assimilation at all the locations as the assimilation window advances in time (Figure 8). Accurate predictions are obtained in the third assimilation step, and those from the fourth match observations almost perfectly. The third and fourth window include, respectively, the central part of the raising limb and peaks of the upstream stations. Note that the match is almost perfect also in the downstream stations where the fourth assimilation

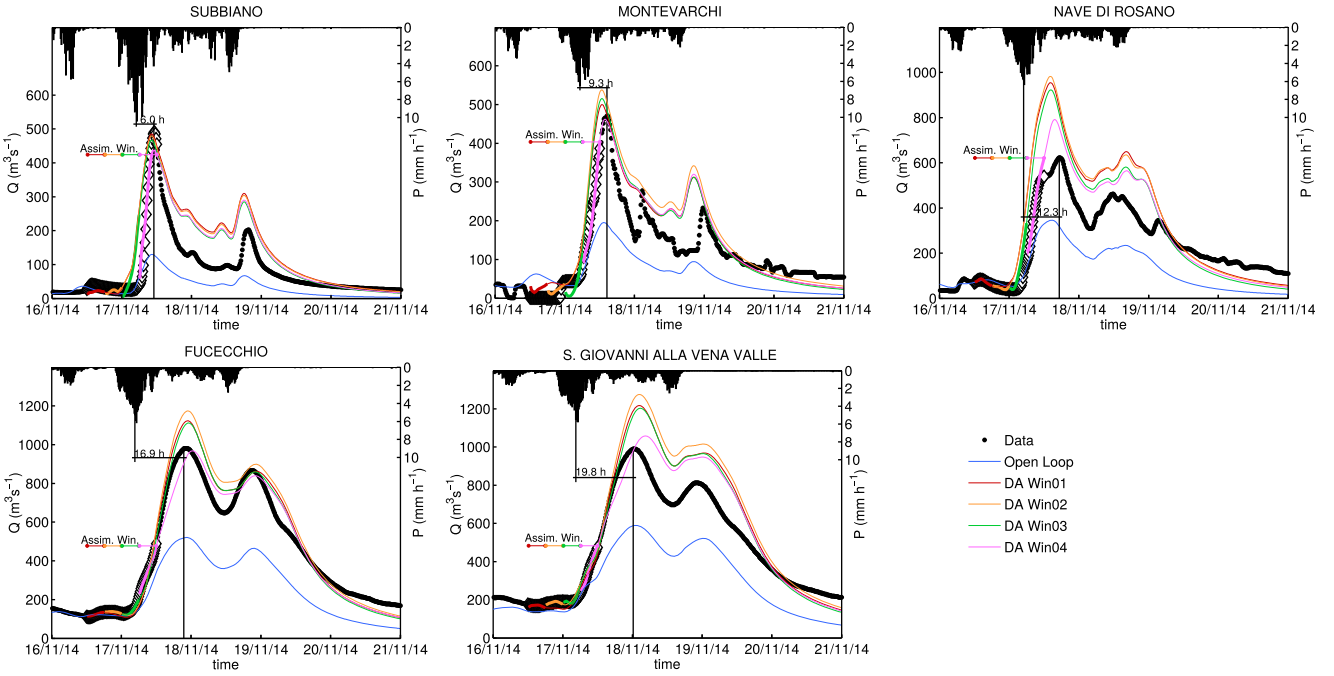

Figure 10. As in Figure 8 but for the high flow event E_{10}. Basin response time (hours) is indicated for each measurement station.

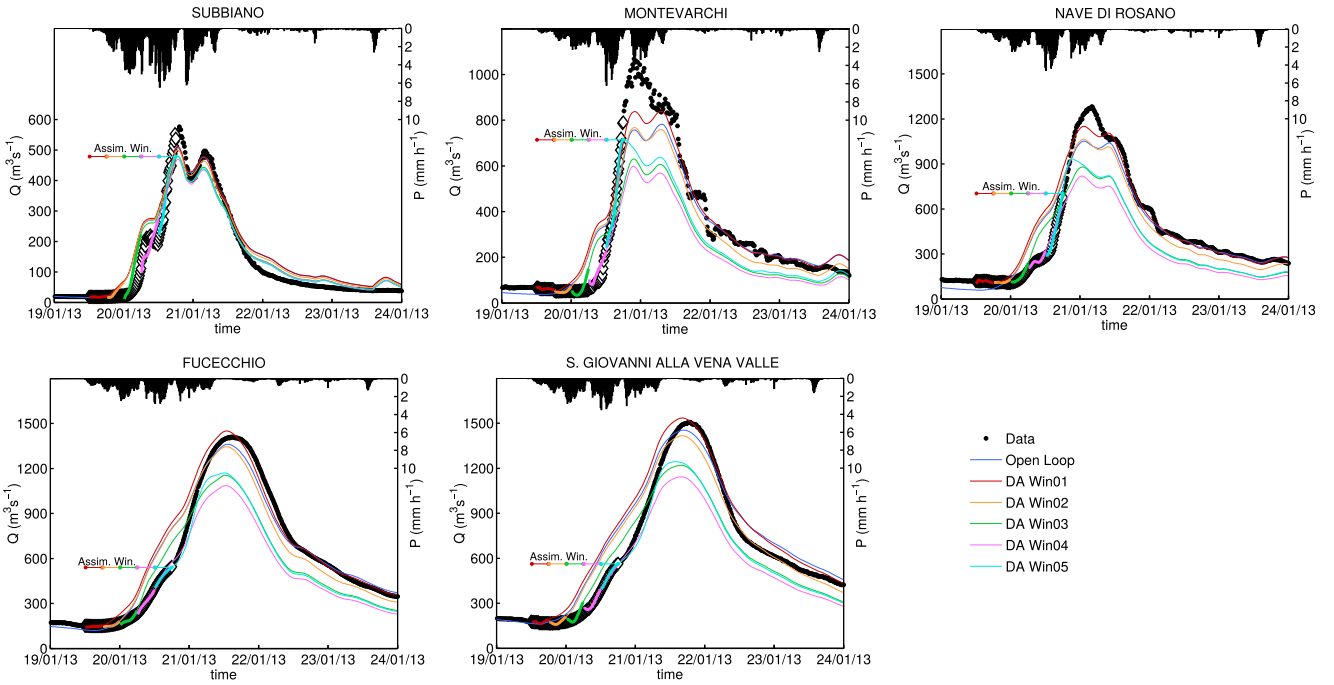

Figure 11. As in Figure 8 but for the high flow event E_{07}.

window does not include the local peak. This behavior is coherent with what already noticed from Figure 6. Namely, the most relevant gain at downstream locations (S.Giovanni alla Vena and Fucecchio) is obtained if upstream peaks, or at least the central part of the rising limb, are included in the assimilation window. Event E_{09} shows an almost opposite impact (Figure 9). Data assimilation initially degrades the accuracy of predictions, especially in terms of peak flow, and mainly at Fucecchio and S.Giovanni alla Vena stations. At this locations, the variational scheme detects an overestimation of the flow during the first two assimilation windows and hence attempts to lower it. The initial overestimation does not correspond to a comparable overestimation of the flood, and corrections imposed by the assimilation eventually worsen the forecasts of the peak. Enhancements are obtained in the third step, whose window corresponds to the central part and the beginning of the rising limb for upstream and downstream locations respectively. Predictions are valuable at all the stations, and excellent at Fucecchio and S.Giovanni alla Vena. The last assimilation includes upstream peaks in the window, and leads to almost perfect predictions at Fucecchio, while performances at S. Giovanni alla Vena slightly deteriorate. The flow is overestimated, with a percentage peak error of about 8.4%, that is nearly equivalent to that of the open loop, although this is of underestimation. The reason could be partially related to errors in flow observations, since data do not show a noticeable increase in flow volume between Fucecchio and S. Giovanni alla Vena. The behavior for event E_{10} (Figure 10) is intermediate. Predictions from data assimilation runs are always better than open loop at all the measurement stations. However, the enhancement is not progressive as in E_{11}. For instance, the second assimilation slightly worsen the forecasts corresponding to the first one. The subsequent assimilation recovers the gap and predictions from the last window are definitely a significant enhancement of the open loop. Differently, in event E_{07} (Figure 11) data assimilation generates a diffuse worsening of forecasting. The open loop anticipates runoff formation in respect to observations, but reproduces quite correctly the peaks at all the measurement stations. The reason is likely that the model does not consider the snowy nature of precipitation, and hence does not reproduce the associated delay in runoff. The assimilation scheme attempts to lower the flow in the early rising limb of the hydrographs, causing a reduction in the total flow volume and in peak flow. The result is that it worsens predictions. A partial remedy can be achieved by proceeding with assimilation (e.g., predictions from the fifth assimilation window). This experiment exemplifies the fact that data assimilation cannot overcome model shortcomings or structural errors, and that an exacerbate forcing of model output toward observations can impact negatively on predictions of a complex dynamical system.

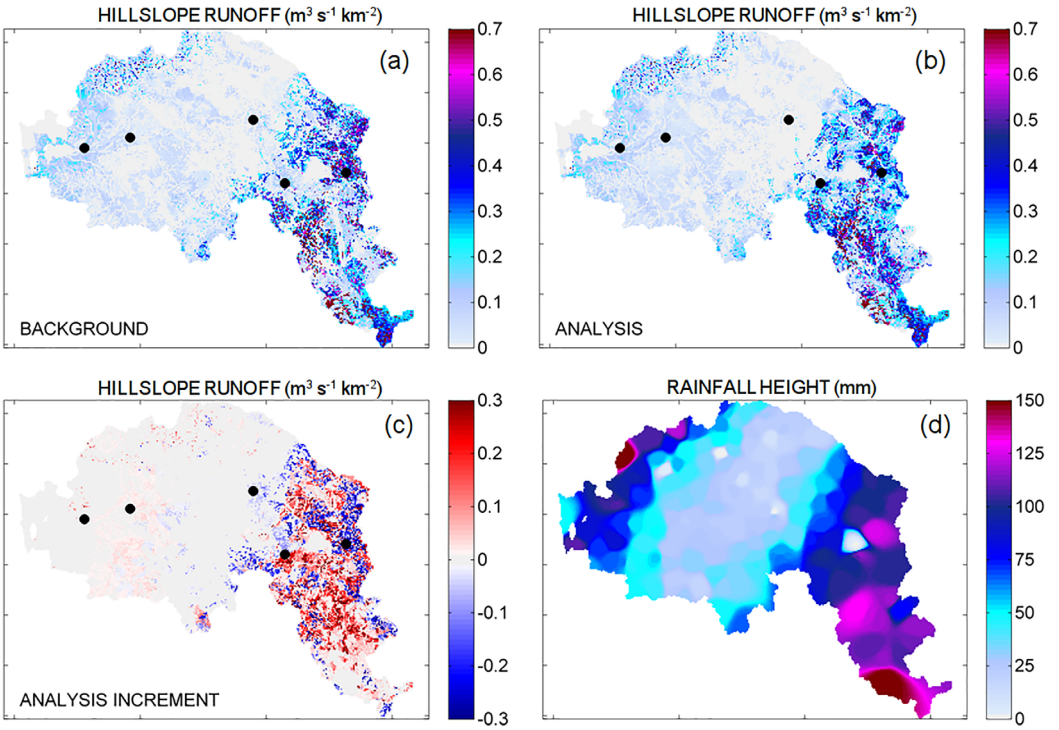

Figure 12. Hillslope runoff ($m^3 s^{-1} km^{-2}$) of the high flow event E_{09} at the final instant of the fourth assimilation window. (a) Is the background map (open loop simulation), (b) is the analysis map (data assimilation simulation), and (c) is the analysis increment (analysis minus background). Black circles indicate the position of the gauge stations. (d) Is the cumulative rainfall height (mm) at the same instant.

Lastly, we show the impact that the assimilation system has on the process of runoff formation. Figure 12 reports maps of hillslope runoff ($m^3 s^{-1} km^{-2}$) and of cumulative rainfall height (mm) at the final instant of the fourth assimilation window of the high flow event E_{09}. In particular, map (a) is the background runoff, i.e., from the open loop run, map (b) is the analysis from the fourth assimilation step and map (c) is the difference between this latter and the background, i.e., the analysis increment. Map (d) is the total rainfall height at the same instant. Note the spatially distributed nature of the correction obtained with the assimilation system, which is mainly concentrated in the area with the highest rainfall height, where uncertainty could be larger. The increment is correctly principally positive, since the open loop simulation suffers underestimation (see Figure 9). However, positive and negative increments are present in adjacent cells in some areas. This happens in cells that, although adjacent, are characterized by significantly different soil properties, and generate considerably dissimilar amounts of hillslope runoff in the open loop run. The assimilation system updates the initial capillary water content in terms of saturation levels at the reach-scale (i.e., selecting the same realization for all the cells contributing to a specific river reach, as explained in more details in section 3.1), smoothing out local differences of saturation. This, in turn, reduces partially the variability of Dunne runoff. In the event shown in Figure 12, referring to the portion of basin upstream to Subbiano station, the spatial variability of the generated hillslope runoff reduces in average of 37% between open loop and analysis. This reduction is estimated by computing the spatial coefficient of variation in each subbasin of the area for both open loop and analysis cumulative hillslope runoff.

The previous analysis shows that the proposed assimilation system has the potential to improve streamflow forecasting on a variety of events, although with different margins. However, some limitations must be underlined. The system acts mainly on runoff formation processes, by updating soil moisture (main impact on Dunne runoff) and f_0 (main impact on Horton runoff). Under extreme conditions of soil saturation (completely dry or fully saturated), this strategy cannot guarantee the spanning of all the state space. In case soil is saturated, no update of f_0 and W_c can increase hillslope runoff. Thus, a possible streamflow underestimation cannot be recovered. Symmetrically, in presence of dry soil and almost null rainfall intermittence, it would not be possible to correct model overestimation of streamflow with only f_0 and W_c as degrees of freedom in the generation of the ensemble. Although such extreme combinations of soil initial

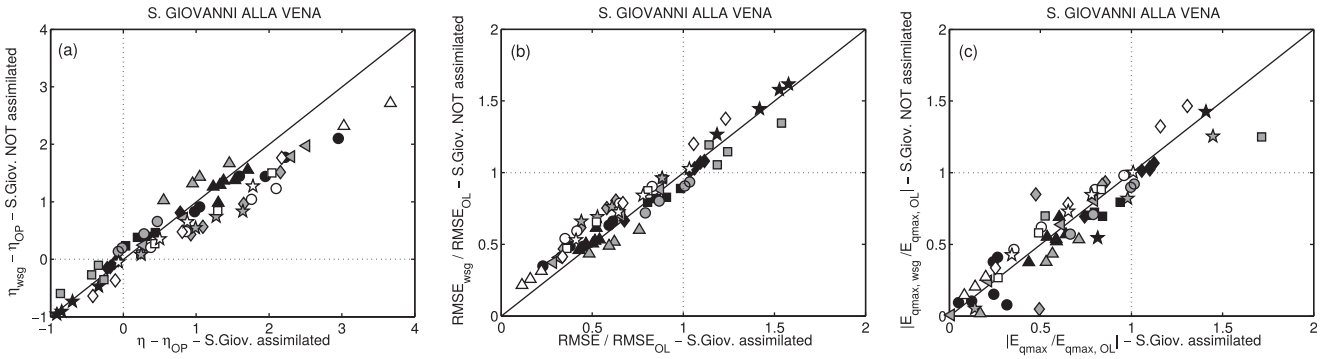

Figure 13. Assimilation system performances obtained at S. Giovanni alla Vena in case data are not assimilated there in comparison to the full-assimilation results. Quantities and symbols are coherent with Figures 4–6.

condition and required correction are not encountered in the examined events, Figure 7b supports the previous rationale, and extends it to more general conditions. The improvement obtained at S. Giovanni alla Vena station, in terms of RMSE reduction and with a lead time of about 10 h, is plotted as a function of the average soil moisture in the contributing area at the beginning of the assimilation procedure. An overall tendency of performances worsening as initial soil saturation grows is detectable. Furthermore, a distinct behavior is present at rather high and low saturation degrees. In the latter case, model overestimation of streamflow cannot be properly corrected, and false alarms events E_{16} and E_{14} maintain a quite relevant RMSE also after the assimilation. With high initial saturation, the worst performances correspond to events that would require an increase of runoff formation (E_{02}, E_{03}, E_{07}). Instead, relevant improvements are obtained when model suffers overestimation and the initial level of saturation is high (E_{08}, E_{12}).

5.1. Performances at Ungauged Locations

As described in the last paragraph of section 4, a second group of 16 experiments is performed to evaluate system performances at ungauged locations. These simulations are identical to the first 16, except that observations are not assimilated at S. Giovanni alla Vena. The obtained results are summarized in Figures 4f, 5f, 6f, and 13 in terms of the 3 statistics employed in this work (η, RMSE, E_{qmax}). In particular, Figure 13 shows performances obtained at S. Giovanni alla Vena in case data are not assimilated there in comparison to the full-assimilation results. Panel (a) plots the difference between η in assimilation runs and in open loop, panel (b) the ratio between RMSE in assimilation runs and open loop, and panel (c) the absolute value of the ratio between error on peak flow in assimilation runs and open loop. The symbols are the same employed in Figures 4–6. Overall, no overturning of capabilities is present, especially in terms of whole hydrograph predictions (η and RMSE). In fact, symbols are grouped around the 1 : 1 line in all the plots. The larger deviation for higher values of $\eta - \eta_{OL}$ is related to the logarithmic character of this measure. Most importantly, it never happens that open loop predictions deteriorate because of not assimilating locally (i.e., no symbols are present in the lower-right quarter of η scatter, or in the upper-left quarter of RMSE and E_{qmax} scatters). Improving or worsening of open loop predictions is maintained from the full-assimilation. Only the level of improvement/degradation changes. In the majority of cases, when data are not assimilated locally, assimilation effectiveness slightly diminishes in respect to the full-assimilation (i.e., most of symbols are below/above the 1 : 1 line in η/RMSE or E_{qmax} scatters). Larger reductions usually corresponds to those events that improve the most in respect to open loop. Thus, the improvements due to the assimilation system remain valuable also when data are not assimilated locally. In some cases, the performances of the system are even better than in the full-assimilation. This happens clearly for events E_{02}, E_{06}, E_{07}, E_{10}, and also for E_{04} and E_{09} in terms of only E_{qmax}. It shows that more information does not corresponds necessarily to a better functioning of the assimilation. When the mismatch between model predictions and observations is due mainly to model structural or parametric errors (and not to an incorrect evaluation of initial conditions), a lower level of constraining can be beneficial. On the basis of the detailed discussion about specific events of the previous section, this is the case for E_{07} and E_{09}. Another situation in which the assimilation system can benefit from reducing the number of assimilation sites, is when the excluded observations are not coherent with those from the other locations (i.e., when the local measurement error is unduly and unexpectedly large).

Lead time-dependency of the changes in system performances in respect to the full-assimilation is illustrated in panel (f) of Figures 4–6. They show the ratio between η, RMSE, E_{qmax} in runs that do not assimilate at S. Giovanni alla Vena and the corresponding value in full-assimilation simulations. The general behavior is that the lack of local assimilation is less influent for lead times in the range 20–30 h, while its impact is increasingly stronger when lead time reduces below 20 h or it increases above 30 h. This is a further indication of the interplay between assimilation lead time, assimilation location and basin response time. Again, system performances decrease more in events where the improvement with respect to the open loop is larger (e.g., E_{08} and E_{15}).

6. Summary and Conclusions

This work presents a new assimilation system of flow data at multiple locations in a distributed hydrologic model. The model MOBIDIC, that is part of the forecasting chain for Arno river in central Italy, is used as operational framework to demonstrate the effectiveness of the developed scheme. The scheme provides optimal estimates of initial flow in the river network, initial capillary water in soil, and rainfall intermittence (parameter f_0) on a distributed basis, using a mixed variational-Monte Carlo approach. Assimilation is realized on sequential windows of 6 h, judging this strategy suitable for an operational usage of the system. We perform a real-time oriented evaluation of the developed system through 16 hindcast experiments in Arno basin. They include both high flow and false alarm events, that are the two crucial situations for flood early warning. The enhancement in flow predictions is assessed through a logarithmic formulation of Nash-Sutcliffe efficiency (η), RMSE, error on peak flow, as well as through hydrographs comparison, taking into account the dependence on lead time.

Results show that the assimilation system can considerably enhance flood forecasts and reduce false alarms, with flow predictions increasingly improving as the assimilation window advances in time. Although specific gains depend on both location and event, in numerous cases a lead time of about 10 h corresponds to a reduction of more than 50% of peak error and an increment of 0.5 or more of η in respect to open loop at all the locations. A lead time of 10 h is comparable with the response time of the basin at the various gauge stations. Shorter forecast horizons lead to more event- and location-independent performances.

The spatially distributed nature of the assimilated information leads to some differences in the behavior between upstream and downstream locations. Overall, the assimilation system becomes more dependent on the specific characteristics of the event as the complexity of the upstream network and the amount of the employed information increase. Furthermore, downstream predictions benefit substantially from an assimilation window that includes upstream peak flows, provided that observations at the various locations are coherent among themselves. Otherwise, the positive impact of the assimilation could be significantly reduced, up to a degradation of model performances. This reveals that, when assimilating streamflow data at multiple locations, the spatial distribution of the gauge stations and the accuracy and mutual coherence of observations can affect substantially the obtainable improvement in predictions. On the other side, the enhancement in proximity of the basin outlet could be satisfactory also without a local assimilation, but using data only from a properly distributed number of upstream stations. This fact is verified by repeating the 16 experiments without assimilating observations at S. Giovanni alla Vena, and comparing performances with the original experiments. As expected, it is found that generally performances slightly reduce, but they remain in line with those of the full-assimilation.

Results show also that, under some conditions, the assimilation system may initially impact negatively on flow predictions. However, it is found that, proceeding with the assimilation, the degradation of the predictions accuracy could be partially recovered, proving that the scheme is robust. The analysis points out that a worsening of predictions may happen when open loop predictions are already accurate, and also when the mismatch between model and observations is due mainly to model shortcoming or structural errors, indicating that the native capabilities of the hydrological model affect significantly the performances of the assimilation system. Namely, the gain obtainable through the assimilation system is limited by model structure, besides possible errors on data, and hence its effectiveness does not depend only from the assimilation scheme itself.

From an operative point of view, the developed assimilation system can be suitable for real-time applications in flood forecasting given its general positive impact on predictions, its robustness and the capability

of improving predictions at downstream ungauged locations. Nevertheless, under specific, but not *a priori* identifiable conditions, a possible negative effect should be taken into account. In addition, in presence of soil almost dry or saturated, the adopted strategy suffers a rigidity that could prevent to fully address the necessary modifications in streamflow.

Further research should investigate the optimal spatial distribution of measurement stations in the river network, and examine in depth the impact of the assimilation on ungauged locations, since this work has provided only a very first insight into the latter topic. Moreover, the influence of the length of the single assimilation window should be better assessed.

Appendix A: Derivation of the Adjoint Model Equations

The penalty functional expressed in equation (20) can be re-written integrating the term $\boldsymbol{\lambda}^T(t)d\boldsymbol{Q}(t)/dt$ by parts:

$$\begin{aligned} J= & \frac{1}{t_1-t_0}\int_{t_0}^{t_1}\left[\left(\boldsymbol{Q}(t)-\boldsymbol{Q}^{obs}(t)\right)^T\frac{\boldsymbol{K_Q}}{2}\left(\boldsymbol{Q}(t)-\boldsymbol{Q}^{obs}(t)\right)\right]dt \\ & +\left[\left(\boldsymbol{Q}(t_1)-\boldsymbol{Q}^{obs}(t_1)\right)^T\frac{\boldsymbol{K_Q}}{2}\left(\boldsymbol{Q}(t_1)-\boldsymbol{Q}^{obs}(t_1)\right)\right] \\ & +\left[\left(\boldsymbol{Q}(t_0)-\boldsymbol{Q}'(t_0)\right)^T\frac{\boldsymbol{K}_{\boldsymbol{Q}_0}}{2}\left(\boldsymbol{Q}(t_0)-\boldsymbol{Q}'(t_0)\right)\right] \\ & +\frac{1}{t_1-t_0}\int_{t_0}^{t_1}\left[\left(\boldsymbol{q_L}(t)-\boldsymbol{q_L}'(t)\right)^T\frac{\boldsymbol{K}_{\boldsymbol{q_L}}}{2}\left(\boldsymbol{q_L}(t)-\boldsymbol{q_L}'(t)\right)\right]dt \\ & +\boldsymbol{\lambda}^T(t)\boldsymbol{Q}(t)\Big|_{t_0}^{t_1}-\int_{t_0}^{t_1}\left[\frac{d\boldsymbol{\lambda}^T(t)}{dt}\boldsymbol{Q}(t)\right]dt-\int_{t_0}^{t_1}\left[\boldsymbol{\lambda}^T(t)\boldsymbol{F}(\boldsymbol{A},\boldsymbol{Q}(t),\boldsymbol{q_L}(t))\right]dt \end{aligned} \tag{A1}$$

In order to minimize J, its first variation δJ must be vanished:

$$\delta J=\frac{\partial J}{\partial \boldsymbol{Q}}\delta\boldsymbol{Q}+\frac{\partial J}{\partial \boldsymbol{Q}_0}\delta\boldsymbol{Q}_0+\frac{\partial J}{\partial \boldsymbol{Q}_1}\delta\boldsymbol{Q}_1+\frac{\partial J}{\partial \boldsymbol{q_L}}\delta\boldsymbol{q_L}=0 \tag{A2}$$

where $\delta\boldsymbol{Q}$ and $\delta\boldsymbol{q_L}$ are the variation of the state and input respectively, and $\delta\boldsymbol{Q}_0$ and $\delta\boldsymbol{Q}_1$ are those corresponding to the initial and final instant of the assimilation window. This general expression can be re-written by making explicit each term:

$$\begin{aligned} \delta J= & \left[\int_{t_0}^{t_1}\left(\frac{\boldsymbol{K_Q}^T\left(\boldsymbol{Q}(t)-\boldsymbol{Q}^{obs}(t)\right)}{t_1-t_0}-\frac{d\boldsymbol{\lambda}(t)}{dt}-\frac{\partial \boldsymbol{F}^T}{\partial \boldsymbol{Q}}\boldsymbol{\lambda}(t)\right)^T dt\right]\delta\boldsymbol{Q} \\ & +\left[\left(\boldsymbol{K}_{\boldsymbol{Q}_0}{}^T\left(\boldsymbol{Q}(t_0)-\boldsymbol{Q}(t_0)'\right)-\boldsymbol{\lambda}(t_0)\right)^T\right]\delta\boldsymbol{Q}_0 \\ & +\left[\left(\boldsymbol{K_Q}^T\left(\boldsymbol{Q}(t_1)-\boldsymbol{Q}^{obs}(t_1)\right)-\boldsymbol{\lambda}(t_1)\right)^T\right]\delta\boldsymbol{Q}_1 \\ & +\left[\int_{t_0}^{t_1}\left(\frac{\boldsymbol{K}_{\boldsymbol{q_L}}{}^T\left(\boldsymbol{q_L}(t)-\boldsymbol{q_L}'(t)\right)}{t_1-t_0}-\frac{\partial \boldsymbol{F}^T}{\partial \boldsymbol{q_L}}\boldsymbol{\lambda}(t)\right)^T dt\right]\delta\boldsymbol{q_L}=0 \end{aligned} \tag{A3}$$

Given independent variations $\delta\boldsymbol{Q}$, $\delta\boldsymbol{Q}_0$, $\delta\boldsymbol{Q}_1$ and $\delta\boldsymbol{q_L}$, the previous condition is equivalent to equations (20), (21), (22) and (23).

Acknowledgments

Authors acknowledge Tuscany Region for supporting the research. In particular, the data sets employed in the analysis have been provided by the Hydrologic Service of Tuscany Region (Servizio Idrologico Regionale, Regione Toscana), and the work has been founded by Tuscany Region through the research project "Attività di ricerca per la mitigazione del rischio idraulico della Regione Toscana," grant CUP-B18C12000300002. The data used in the paper are available upon request (fabio.castelli@unifi.it). The authors thank the three anonymous reviewers for their valuable comments.

References

Abaza, M., C. Garneau, and F. Anctil (2014), Comparison of sequential and variational streamflow assimilation techniques for short-term hydrological forecasting, *J. Hydrol. Eng.*, *20*(2), 04014042, doi:10.1061/(ASCE)HE.1943-5584.0001013.

Andreadis, K. M., E. A. Clark, D. P. Lettenmaier, and D. E. Alsdorf (2007), Prospects for river discharge and depth estimation through assimilation of swath-altimetry into a raster-based hydrodynamics model, *Geophys. Res. Lett.*, *34*, L10403, doi:10.1029/2007GL029721.

Arulampalam, M. S., S. Maskell, N. Gordon, and T. Clapp (2002), A tutorial on particle filters for online nonlinear/non-Gaussian Bayesian tracking, *IEEE Trans. Signal Process.*, *50*(2), 174–188, doi:10.1109/78.978374.

Bennett, A. F. (1992), *Inverse Methods in Physical Oceanography*, Cambridge Univ. Press, Cambridge.

Brocca, L., F. Melone, T. Moramarco, W. Wagner, V. Naeimi, Z. Bartalis, and S. Hasenauer (2010), Improving runoff prediction through the assimilation of the ASCAT soil moisture product, *Hydrol. Earth Syst. Sci.*, *14*(10), 1881–1893, doi:10.5194/hess-14-1881-2010.

Brocca, L., T. Moramarco, F. Melone, W. Wagner, S. Hasenauer, and S. Hahn (2012), Assimilation of surface- and root-zone ASCAT soil moisture products into rainfall–runoff modeling, *IEEE Trans. Geosci. Remote Sens.*, *50*(7), 2542–2555, doi:10.1109/TGRS.2011.2177468.

Brooks, R. H., and A. T. Corey (1964), Hydraulic properties of porous media and their relation to drainage design, *Trans. ASAE*, *7*(1), 26–28.

Campo, L., F. Caparrini, and F. Castelli (2006), Use of multi-platform, multi-temporal remote-sensing data for calibration of a distributed hydrological model: An application in the Arno basin, Italy, *Hydrol. Processes*, *20*(13), 2693–2712, doi:10.1002/hyp.6061.

Campo, L., F. Castelli, D. Entekhabi, and F. Caparrini (2013), Analysis of a two-year meteorological dataset produced on Italian territory with a coupling procedure between a limited area atmospheric model and a sequential MSG-SEVIRI LST assimilation scheme, *Int. J. Remote Sens.*, *34*(9-10), 3561–3586, doi:10.1080/01431161.2012.716535.

Caparrini, F., F. Castelli, and D. Entekhabi (2004a), Estimation of surface turbulent fluxes through assimilation of radiometric surface temperature sequences, *J. Hydrometeorol.*, *5*(1), 145–159, doi:10.1175/1525-7541(2004)005<0145:EOSTFT>2.0.CO;2.

Caparrini, F., F. Castelli, and D. Entekhabi (2004b), Variational estimation of soil and vegetation turbulent transfer and heat flux parameters from sequences of multisensor imagery, *Water Resour. Res.*, *40*, W12515, doi:10.1029/2004WR003358.

Carsell, K. M., N. D. Pingel, and D. T. Ford (2004), Quantifying the benefit of a flood warning system, *Nat. Hazards Rev.*, *5*(3), 131–140, doi:10.1061/(ASCE)1527-6988(2004)5:3(131).

Castelli, F. (1996), A simplified stochastic model for infiltration into a heterogeneous soil forced by random precipitation, *Adv. Water Resour.*, *19*(3), 133–144, doi:10.1016/0309-1708(95)00041-0.

Castelli, F., D. Entekhabi, and E. Caporali (1999), Estimation of surface heat flux and an index of soil moisture using adjoint-state surface energy balance, *Water Resour. Res.*, *35*(10), 3115–3125, doi:10.1029/1999WR900140.

Castelli, F., G. Menduni, and B. Mazzanti (2009), A distributed package for sustainable water management: A case study in the Arno basin, *IAHS Publ.*, *327*, 52–61.

Castillo, A., F. Castelli, and D. Entekhabi (2015), Gravitational and capillary soil moisture dynamics for distributed hydrologic models, *Hydrol. Earth Syst. Sci.*, *19*(4), 1857–1869, doi:10.5194/hess-19-1857-2015.

Chen, J., W. Zhang, J. Gao, and K. Cao (2012), Assimilating multi-site measurements for semi-distributed hydrological model updating, *Quat. Int.*, *282*, 122–129, doi:10.1016/j.quaint.2012.01.030.

Cheng, Q.-B., X. Chen, C.-Y. Xu, C. Reinhardt-Imjela, and A. Schulte (2014), Improvement and comparison of likelihood functions for model calibration and parameter uncertainty analysis within a Markov chain Monte Carlo scheme, *J. Hydrol.*, *519*, 2202–2214.

Clark, M. P., A. G. Slater, A. P. Barrett, L. E. Hay, G. J. McCabe, B. Rajagopalan, and G. H. Leavesley (2006), Assimilation of snow covered area information into hydrologic and land-surface models, *Adv. Water Resour.*, *29*(8), 1209–1221, doi:10.1016/j.advwatres.2005.10.001.

Clark, M. P., D. E. Rupp, R. A. Woods, X. Zheng, R. P. Ibbitt, A. G. Slater, J. Schmidt, and M. J. Uddstrom (2008), Hydrological data assimilation with the ensemble Kalman filter: Use of streamflow observations to update states in a distributed hydrological model, *Adv. Water Resour.*, *31*(10), 1309–1324, doi:10.1016/j.advwatres.2008.06.005.

Coustau, M., S. Ricci, V. Borrell-Estupina, C. Bouvier, and O. Thual (2013), Benefits and limitations of data assimilation for discharge forecasting using an event-based rainfall-runoff model, *Nat. Hazards Earth Syst. Sci.*, *13*, 583, doi:10.5194/nhess-13-583-2013.

Coustau, M., F. Rousset-Regimbeau, G. Thirel, F. Habets, B. Janet, E. Martin, C. de Saint-Aubin, and J.-M. Soubeyroux (2015), Impact of improved meteorological forcing, profile of soil hydraulic conductivity and data assimilation on an operational Hydrological Ensemble Forecast System over France, *J. Hydrol.*, *525*, 781–792, doi:10.1016/j.jhydrol.2015.04.022.

Crow, W., and D. Ryu (2009), A new data assimilation approach for improving runoff prediction using remotely-sensed soil moisture retrievals, *Hydrol. Earth Syst. Sci.*, *13*(1), 1–16, doi:10.5194/hess-13-1-2009.

DeChant, C. M., and H. Moradkhani (2011), Improving the characterization of initial condition for ensemble streamflow prediction using data assimilation, *Hydrol. Earth Syst. Sci.*, *15*(11), 3399–3410, doi:10.5194/hess-15-3399-2011.

DeChant, C. M., and H. Moradkhani (2012), Examining the effectiveness and robustness of sequential data assimilation methods for quantification of uncertainty in hydrologic forecasting, *Water Resour. Res.*, *48*, W04518, doi:10.1029/2011WR011011.

De Lannoy, G. J., R. H. Reichle, K. R. Arsenault, P. R. Houser, S. Kumar, N. E. Verhoest, and V. Pauwels (2012), Multiscale assimilation of Advanced Microwave Scanning Radiometer–EOS snow water equivalent and Moderate Resolution Imaging Spectroradiometer snow cover fraction observations in northern Colorado, *Water Resour. Res.*, *48*, W01522, doi:10.1029/2011WR010588.

Ding, Y., and S. S. Wang (2005), Identification of Manning's roughness coefficients in channel network using adjoint analysis, *Int. J. Comput. Fluid Dyn.*, *19*(1), 3–13.

Dingman, S. L. (2008), *Physical Hydrology*, Waveland Press, Long Grove.

Evensen, G. (1994), Sequential data assimilation with a nonlinear quasi-geostrophic model using Monte Carlo methods to forecast error statistics, *J. Geophys. Res.*, *99*(C5), 10,143–10,162, doi:10.1029/94JC00572.

Fang, H., S. Liang, and G. Hoogenboom (2011), Integration of MODIS LAI and vegetation index products with the CSM–CERES–Maize model for corn yield estimation, *Int. J. Remote Sens.*, *32*(4), 1039–1065, doi:10.1080/01431160903505310.

Gardin, L. (2014), Hydrologic characterization of Tuscany soils for the MOBIDIC model, [in Italian], technical report, Tuscany Region. [Available at http://www.regione.toscana.it/documents/11974914/12673503/COMPORTAMENTO_IDROLOGICO_DEI_SUOLI_RT.pdf/d9ec21b1-341b-44d7-ac9a-862fa4949433.]

Ines, A. V., N. N. Das, J. W. Hansen, and E. G. Njoku (2013), Assimilation of remotely sensed soil moisture and vegetation with a crop simulation model for maize yield prediction, *Remote Sens. Environ.*, *138*, 149–164, doi:10.1016/j.rse.2013.07.018.

Irmak, A., and B. Kamble (2009), Evapotranspiration data assimilation with genetic algorithms and SWAP model for on-demand irrigation, *Irrig. Sci.*, *28*(1), 101–112, doi:10.1007/s00271-009-0193-9.

Kalnay, E. (2003), *Atmospheric Modeling, Data Assimilation and Predictability*, Cambridge Univ. Press, Cambridge.

Komma, J., G. Blöschl, and C. Reszler (2008), Soil moisture updating by Ensemble Kalman Filtering in real-time flood forecasting, *J. Hydrol.*, *357*(3), 228–242, doi:10.1016/j.jhydrol.2008.05.020.

Kumar, S. V., R. H. Reichle, R. D. Koster, W. T. Crow, and C. D. Peters-Lidard (2009), Role of subsurface physics in the assimilation of surface soil moisture observations, *J. Hydrometeorol.*, *10*(6), 1534–1547, doi:10.1175/2009JHM1134.1.

Laiolo, P., et al. (2015), Impact of different satellite soil moisture products on the predictions of a continuous distributed hydrological model, *Int. J. Appl. Earth Obs.*, *48*, 131–145, doi:10.1016/j.jag.2015.06.002.

Lee, H., D.-J. Seo, and V. Koren (2011), Assimilation of streamflow and in situ soil moisture data into operational distributed hydrologic models: Effects of uncertainties in the data and initial model soil moisture states, *Adv. Water Resour.*, *34*(12), 1597–1615, doi:10.1016/j.advwatres.2011.08.012.

Lee, H., D.-J. Seo, Y. Liu, V. Koren, P. McKee, and R. Corby (2012), Variational assimilation of streamflow into operational distributed hydrologic models: Effect of spatiotemporal scale of adjustment, *Hydrol. Earth Syst. Sci.*, *16*(7), 2233–2251, doi:10.5194/hess-16-2233-2012.
Li, B., D. Toll, X. Zhan, and B. Cosgrove (2012), Improving estimated soil moisture fields through assimilation of AMSR-E soil moisture retrievals with an ensemble Kalman filter and a mass conservation constraint, *Hydrol. Earth Syst. Sci.*, *16*(1), 105–119, doi:10.5194/hess-16-105-2012.
Li, Y., D. Ryu, A. W. Western, and Q. Wang (2015), Assimilation of stream discharge for flood forecasting: Updating a semidistributed model with an integrated data assimilation scheme, *Water Resour. Res.*, *51*, 3238–3258, doi:10.1002/2014WR016667.
Liston, G. E., and C. A. Hiemstra (2008), A simple data assimilation system for complex snow distributions (SnowAssim), *J. Hydrometeorol.*, *9*(5), 989–1004, doi:10.1175/2008JHM871.1.
Liu, Y., and H. V. Gupta (2007), Uncertainty in hydrologic modeling: Toward an integrated data assimilation framework, *Water Resour. Res.*, *43*, W07401, doi:10.1029/2006WR005756.
Liu, Y., et al. (2012), Advancing data assimilation in operational hydrologic forecasting: Progresses, challenges, and emerging opportunities, *Hydrol. Earth Syst. Sci.*, *16*(10), 3863–3887, doi:10.5194/hess-16-3863-2012.
Margulis, S. A., and D. Entekhabi (2001), A coupled land surface-boundary layer model and its adjoint, *J. Hydrometeorol.*, *2*(3), 274–296, doi:10.1175/1525-7541(2001)002<0274:ACLSBL>2.0.CO;2.
Margulis, S. A., and D. Entekhabi (2003), Variational assimilation of radiometric surface temperature and reference-level micrometeorology into a model of the atmospheric boundary layer and land surface, *Mon. Weather Rev.*, *131*(7), 1272–1288, doi:10.1175/1520-0493(2003)131<1272:VAORST>2.0.CO;2.
Margulis, S. A., and D. Entekhabi (2004), Boundary-layer entrainment estimation through assimilation of radiosonde and micrometeorological data into a mixed-layer model, *Boundary Layer Meteorol.*, *110*(3), 405–433, doi:10.1023/B:BOUN.0000007221.53446.46.
Mazzoleni, M., L. Alfonso, J. Chacon-Hurtado, and D. Solomatine (2015), Assimilating uncertain, dynamic and intermittent streamflow observations in hydrological models, *Adv. Water Resour.*, *83*, 323–339, doi:10.1016/j.advwatres.2015.07.004.
McMillan, H., E. Hreinsson, M. Clark, S. Singh, C. Zammit, and M. Uddstrom (2013), Operational hydrological data assimilation with the recursive ensemble Kalman filter, *Hydrol. Earth Syst. Sci.*, *17*(1), 21–38, doi:10.5194/hess-17-21-2013.
Molinari, D., and J. Handmer (2011), A behavioural model for quantifying flood warning effectiveness, *J. Flood Risk Manage.*, *4*(1), 23–32, doi:10.1111/j.1753-318X.2010.01086.x.
Moradkhani, H., K.-L. Hsu, H. Gupta, and S. Sorooshian (2005), Uncertainty assessment of hydrologic model states and parameters: Sequential data assimilation using the particle filter, *Water Resour. Res.*, *41*, W05012, doi:10.1029/2004WR003604.
Moradkhani, H., C. M. DeChant, and S. Sorooshian (2012), Evolution of ensemble data assimilation for uncertainty quantification using the particle filter-Markov chain Monte Carlo method, *Water Resour. Res.*, *48*, W12520, doi:10.1029/2012WR012144.
Noh, S., Y. Tachikawa, M. Shiiba, and S. Kim (2011), Applying sequential Monte Carlo methods into a distributed hydrologic model: Lagged particle filtering approach with regularization, *Hydrol. Earth Syst. Sci.*, *15*(10), 3237–3251, doi:10.5194/hess-15-3237-2011.
Noh, S. J., Y. Tachikawa, M. Shiiba, and S. Kim (2013), Ensemble Kalman filtering and particle filtering in a lag-time window for short-term streamflow forecasting with a distributed hydrologic model, *J. Hydrol. Eng.*, *18*(12), 1684–1696, doi:10.1061/(ASCE)HE.1943-5584.0000751.
Noh, S. J., O. Rakovec, A. H. Weerts, and Y. Tachikawa (2014), On noise specification in data assimilation schemes for improved flood forecasting using distributed hydrological models, *J. Hydrol.*, *519*, 2707–2721, doi:10.1016/j.jhydrol.2014.07.049.
Pagano, T. C., et al. (2014), Challenges of operational river forecasting, *J. Hydrometeorol.*, *15*(4), 1692–1707, doi:10.1175/JHM-D-13-0188.1.
Pappenberger, F., H. L. Cloke, D. J. Parker, F. Wetterhall, D. S. Richardson, and J. Thielen (2015), The monetary benefit of early flood warnings in Europe, *Environ. Sci. Policy*, *51*, 278–291, doi:10.1016/j.envsci.2015.04.016.
Pasetto, D., M. Camporese, and M. Putti (2012), Ensemble Kalman filter versus particle filter for a physically-based coupled surface–subsurface model, *Adv. Water Resour.*, *47*, 1–13, doi:10.1016/j.advwatres.2012.06.009.
Pauwels, V., and G. J. De Lannoy (2009), Ensemble-based assimilation of discharge into rainfall-runoff models: A comparison of approaches to mapping observational information to state space, *Water Resour. Res.*, *45*, W08428, doi:10.1029/2008WR007590.
Pauwels, V. R., R. Hoeben, N. E. Verhoest, and F. P. De Troch (2001), The importance of the spatial patterns of remotely sensed soil moisture in the improvement of discharge predictions for small-scale basins through data assimilation, *J. Hydrol.*, *251*(1), 88–102, doi:10.1016/S0022-1694(01)00440-1.
Pipunic, R., J. Walker, and A. Western (2008), Assimilation of remotely sensed data for improved latent and sensible heat flux prediction: A comparative synthetic study, *Remote Sens. Environ.*, *112*(4), 1295–1305, doi:10.1016/j.rse.2007.02.038.
Rafieeinasab, A., D.-J. Seo, H. Lee, and S. Kim (2014), Comparative evaluation of maximum likelihood ensemble filter and ensemble Kalman filter for real-time assimilation of streamflow data into operational hydrologic models, *J. Hydrol.*, *519*, 2663–2675, doi:10.1016/j.jhydrol.2014.06.052.
Rakovec, O., A. Weerts, P. Hazenberg, P. Torfs, and R. Uijlenhoet (2012), State updating of a distributed hydrological model with Ensemble Kalman Filtering: Effects of updating frequency and observation network density on forecast accuracy, *Hydrol. Earth Syst. Sci.*, *16*(9), 3435–3449, doi:10.5194/hess-16-3435-2012.
Rakovec, O., A. Weerts, J. Sumihar, and R. Uijlenhoet (2015), Operational aspects of asynchronous filtering for flood forecasting, *Hydrol. Earth Syst. Sci.*, *19*(6), 2911–2924, doi:10.5194/hess-19-2911-2015.
Reichle, R. H. (2008), Data assimilation methods in the Earth sciences, *Adv. Water Resour.*, *31*(11), 1411–1418, doi:j.advwatres.2008.01.001.
Reichle, R. H., D. Entekhabi, and D. B. McLaughlin (2001), Downscaling of radio brightness measurements for soil moisture estimation: A four-dimensional variational data assimilation approach, *Water Resour. Res.*, *37*(9), 2353–2364, doi:10.1029/2001WR000475.
Reichle, R. H., R. D. Koster, P. Liu, S. P. Mahanama, E. G. Njoku, and M. Owe (2007), Comparison and assimilation of global soil moisture retrievals from the Advanced Microwave Scanning Radiometer for the Earth Observing System (AMSR-E) and the Scanning Multichannel Microwave Radiometer (SMMR), *J. Geophys. Res.*, *112*, D09108, doi:10.1029/2006JD008033.
Reichle, R. H., W. T. Crow, and C. L. Keppenne (2008), An adaptive ensemble Kalman filter for soil moisture data assimilation, *Water Resour. Res.*, *44*, W03423, doi:10.1029/2007WR006357.
Reichle, R. H., S. V. Kumar, S. P. Mahanama, R. D. Koster, and Q. Liu (2010), Assimilation of satellite-derived skin temperature observations into land surface models, *J. Hydrometeorol.*, *11*(5), 1103–1122, doi:10.1175/2010JHM1262.1.
Sahoo, A. K., G. J. De Lannoy, R. H. Reichle, and P. R. Houser (2013), Assimilation and downscaling of satellite observed soil moisture over the Little River Experimental Watershed in Georgia, USA, *Adv. Water Resour.*, *52*, 19–33, doi:j.advwatres.2012.08.007.
Salamon, P., and L. Feyen (2009), Assessing parameter, precipitation, and predictive uncertainty in a distributed hydrological model using sequential data assimilation with the particle filter, *J. Hydrol.*, *376*(3), 428–442.
Salvucci, G. D. (1993), An approximate solution for steady vertical flux of moisture through an unsaturated homogeneous soil, *Water Resour. Res.*, *29*(11), 3749–3753, doi:10.1029/93WR02068.

Schuurmans, J., P. Troch, A. Veldhuizen, W. Bastiaanssen, and M. Bierkens (2003), Assimilation of remotely sensed latent heat flux in a distributed hydrological model, *Adv. Water Resour.*, *26*(2), 151–159, doi:10.1016/S0309-1708(02)00089-1.

Schuurmans, J., F. Van Geer, and M. Bierkens (2011), Remotely sensed latent heat fluxes for model error diagnosis: A case study, *Hydrol. Earth Syst. Sci.*, *15*(3), 759–769, doi:10.5194/hess-15-759-2011.

Seo, D.-J., V. Koren, and N. Cajina (2003), Real-time variational assimilation of hydrologic and hydrometeorological data into operational hydrologic forecasting, *J. Hydrometeorol.*, *4*(3), 627–641, doi:10.1175/1525-7541(2003)004<0627:RVAOHA>2.0.CO;2.

Seo, D.-J., L. Cajina, R. Corby, and T. Howieson (2009), Automatic state updating for operational streamflow forecasting via variational data assimilation, *J. Hydrol.*, *367*(3), 255–275, doi:10.1016/j.jhydrol.2009.01.019.

Sini, F., G. Boni, F. Caparrini, and D. Entekhabi (2008), Estimation of large-scale evaporation fields based on assimilation of remotely sensed land temperature, *Water Resour. Res.*, *44*, W06410, doi:10.1029/2006WR005574.

Su, H., Z.-L. Yang, R. E. Dickinson, C. R. Wilson, and G.-Y. Niu (2010), Multisensor snow data assimilation at the continental scale: The value of Gravity Recovery and Climate Experiment terrestrial water storage information, *J. Geophys. Res.*, *115*, D10104, doi:10.1029/2009JD013035.

Thirel, G., E. Martin, J.-F. Mahfouf, S. Massart, S. Ricci, and F. Habets (2010a), A past discharges assimilation system for ensemble streamflow forecasts over France–Part 1: Description and validation of the assimilation system, *Hydrol. Earth Syst. Sci.*, *14*, 1623–1637, doi:10.5194/hess-14-1623-2010.

Thirel, G., E. Martin, J.-F. Mahfouf, S. Massart, S. Ricci, F. Regimbeau, and F. Habets (2010b), A past discharge assimilation system for ensemble streamflow forecasts over France–Part 2: Impact on the ensemble streamflow forecasts, *Hydrol. Earth Syst. Sci.*, *14*, 1639–1653, doi:10.5194/hess-14-1639-2010.

UNISDR (2002), Guidelines for reducing flood losses, *Tech. Rep. DRR7639*, United Nations. [Available at http://www.unisdr.org/files/558_7639.pdf.]

Van den Hurk, B., and A. Holtslag (1997), On the bulk parameterization of surface fluxes for various conditions and parameter ranges, *Boundary Layer Meteorol.*, *82*(1), 119–133, doi:10.1023/A:1000245600901.

Vrugt, J. A., H. V. Gupta, B. Nualláin, and W. Bouten (2006), Real-time data assimilation for operational ensemble streamflow forecasting, *J. Hydrometeorol.*, *7*(3), 548–565, doi:10.1175/JHM504.1.

Weerts, A. H., and G. Y. El Serafy (2006), Particle filtering and ensemble Kalman filtering for state updating with hydrological conceptual rainfall-runoff models, *Water Resour. Res.*, *42*, W09403, doi:10.1029/2005WR004093.

Xie, X., and D. Zhang (2010), Data assimilation for distributed hydrological catchment modeling via ensemble Kalman filter, *Adv. Water Resour.*, *33*(6), 678–690, doi:10.1016/j.advwatres.2010.03.012.

Yan, H., and H. Moradkhani (2016), Combined assimilation of streamflow and satellite soil moisture with the particle filter and geostatistical modeling, *Adv. Water Resour.*, *94*, 364–378, doi:10.1016/j.advwatres.2016.06.002.

Yang, J., F. Castelli, and Y. Chen (2014a), Multiobjective sensitivity analysis and optimization of distributed hydrologic model MOBIDIC, *Hydrol. Earth Syst. Sci.*, *18*(10), 4101–4112, doi:10.5194/hess-18-4101-2014.

Yang, J., D. Entekhabi, F. Castelli, and L. Chua (2014b), Hydrologic response of a tropical watershed to urbanization, *J. Hydrol.*, *517*, 538–546, doi:10.1016/j.jhydrol.2014.05.053.